Petrology and Geochemistry of Cretaceous Ultramafic Volcanics from Eastern Kamchatka

Article *in* Journal of Petrology · June 1995

DOI: 10.1093/petrology/36.3.637

4 authors, including:

Vadim S. Kamenetsky
University of Tasmania
413 PUBLICATIONS **13,151** CITATIONS
SEE PROFILE

Alexander V Sobolev
Université Grenoble Alpes
262 PUBLICATIONS **10,327** CITATIONS
SEE PROFILE

J.-L. Joron
Paris Diderot University
305 PUBLICATIONS **11,878** CITATIONS
SEE PROFILE

JOURNAL OF PETROLOGY | VOLUME 36 | NUMBER 3 | PAGES 637–662 | 1995

V. S. KAMENETSKY[1]*, A. V. SOBOLEV[1], J.-L. JORON[2] AND M. P. SEMET[3]
[1]VERNADSKY INSTITUTE OF GEOCHEMISTRY, RUSSIAN ACADEMY OF SCIENCES, KOSYGIN STR 19, MOSCOW 117975, RUSSIA
[2]GROUPE DES SCIENCES DE LA TERRE, LABORATOIRE PIERRE SÜE, CEN SACLAY, 91191 GIF SUR YVETTE CÉDEX, FRANCE
[3]LABORATOIRE DE GÉOCHIMIE COMPARÉE ET SYSTEMATIQUE, URA X-01758 CNRS, 75252 PARIS CÉDEX 05, FRANCE

Petrology and Geochemistry of Cretaceous Ultramafic Volcanics from Eastern Kamchatka

The origin, evolution and primary melt compositions of late Cretaceous high-K ultramafic volcanics and associated basalts of Eastern Kamchatka are discussed on the basis of a study of the mineralogy and geochemistry of the rocks and magmatic inclusions in phenocrysts. The exceptionally primitive composition of the phenocryst assemblage [olivine—Fo_{89-95}, Cr-spinel—Cr/(Cr + Al) up to 85] provides direct evidence of the mantle origin of primary melts, which were highly magnesian compositions (MgO 19–24 wt %). The rocks and melts are characterized by strong high field strength element (HFSE) depletion in comparison with rare earth elements, and high and variable levels of enrichment in large ion lithophile elements (LILE), P, K and H_2O (0·6–1·2 wt % in picritic to basaltic melts). ε_{Nd} values lie in a narrow range (+10·7 to +9·1), typical of N-MORB (mid-ocean ridge basalt), but $^{87}Sr/^{86}Sr$ (0·70316–0·70358) is slightly displaced from the mantle array. High-K ultramafic melts from Kamchatka are considered as a new magma type within the island-arc magmatic spectrum; basaltic members of the suite resemble arc shoshonites. The primary melts were produced under high-pressure (30–50 kbar) and high-temperature (1500–1700°C) conditions by partial melting of a refractory peridotitic mantle.

KEY WORDS: *Kamchatka; Late Cretaceous magmatism; ultramafic volcanics; shoshonites.*

INTRODUCTION

Information concerning the nature and variety of primary magmas in island arcs is scarce, and the conditions of their generation and source components remain controversial. The major reason for this is that primitive arc lavas are rare, with inferred liquid compositions with >8% MgO being exceptionally uncommon, especially for tholeiitic arc magmas. Most data on primitive arc lavas exist for boninites from the Western Pacific: Cape Vogel, Papua New Guinea (Walker & Cameron, 1983), Tonga (Falloon *et al.*, 1989; Sobolev & Danyushevsky, 1994) and Hunter Fracture Zone (Sigurdsson *et al.*, 1993); another well-documented locality of primitive boninites is Troodos, Cyprus (e.g. Sobolev *et al.*, 1993). Primitive arc tholeiites spatially associated with boninites have been found in Lower Pillow Lavas of Cyprus (Sobolev *et al.*, 1993) and the Hunter Fracture Zone between Vanuatu and Fiji in the southwest Pacific (Sigurdsson *et al.*, 1993). Data on primitive high-K or calc-alkaline island-arc suites come mostly from the circum-Pacific region: Solomon Islands (Ramsay *et al.*, 1984), Vanuatu (Eggins, 1993) and Jorullo volcano, Mexico (Luhr & Carmichael, 1985). This study concentrated on determining the nature of the parent magma of an alkaline (high-K) suite from the poorly known Kamchatka arc.

Phanerozoic high-Mg (MgO >18%) parental magmas have been demonstrated for Gorgona Island komatiites (Echeverría, 1980), the meimechites of Siberia (Sobolev & Slutsky, 1984; Sobolev *et al.*, 1992), Tongan boninites (Sobolev & Danyushevsky, 1994) and the Upper Pillow Lavas of Cyprus (Sobolev *et al.*, 1993), and are argued to have been parental to boninites from Cape Vogel, Papua New Guinea (Walker & Cameron, 1983) and the Lachlan Foldbelt in SE Australia (Crawford, 1980), and picrites from New Georgia in the Solomon Islands (Ramsay *et al.*, 1984) and Ambae (Aoba) volcano in Vanuatu (Eggins, 1993). Here, we argue that the

*Corresponding author.
Present address: Department of Geology, University of Tasmania, GPO Box 252C, Hobart, Tas., Australia

primary magma of the Late Cretaceous ultramafic lavas of Kamchatka may have had up to 24 wt% MgO. A detailed mineralogical, geochemical and isotope study of these rocks, together with an experimental investigation of melt inclusions, was carried out to contribute to understanding of the P–T conditions of island-arc magma generation, and in particular, of alkaline arc magmas. We summarize published Russian literature (e.g. Erlikh *et al.*, 1971; Seliverstov, 1978; Markovsky & Rotman, 1981; Sobolev *et al.*, 1990; Kamenetsky *et al.*, 1991, 1993) and show that the Eastern Kamchatka ultramafic lavas are very unusual high-K, arc-type lavas, generated by very high-pressure partial melting of peridotitic mantle.

Magmatic inclusions in phenocrysts provide a glimpse of a particular evolutionary stage of a magma, as sampled at a particular time, place and physical and chemical conditions. From melt-inclusion study, combined with suitable theoretical and numerical treatment, the composition and temperature of the primary melt may be successfully reconstructed. This work also demonstrates the utility of melt-inclusion studies (including ion-microprobe analysis) in establishing parental and primary magma types, especially in ancient arc terranes where the rocks have undergone extensive post-magmatic alteration.

REGIONAL SETTING

The ultramafic volcanics of Kamchatka occur within neotectonic uplifted blocks of the Eastern Kamchatka structural zone (Fig. 1) including the Valaginsky Range (VR), Tumrok Range (TR) and Sharomsky Mis (SHR) (Zinkevich *et al.*, 1989, 1990, 1991; Kamenetsky *et al.*, 1991, 1993). This zone, elongated north-northeast along the Pacific coast of the Kamchatka peninsula, forms the basement of the northern part of the Cenozoic Kurile–Kamchatka island arc. It is composed of Cretaceous–lower Paleogene volcanic and volcano-sedimentary terranes, originally generated in island-arc, back-arc and forearc basin settings (Zinkevich *et al.*, 1991). The structure and stratigraphy of the Eastern Kamchatka structural zone are complex and as yet poorly understood. The occurrence of ultramafic volcanics in the relatively undisturbed succession of the TR is the best studied and can be used for further reconstruction of the pre-Cenozoic tectonic and magmatic evolution of the region.

The Tumrok block of late Cretaceous to early Paleogene rocks is located at the intersection of two large NE–SW neotectonic fault systems. It is separated by a major, steeply dipping fault-zone from the graben-like Cenozoic Central Kamchatka rift to the west. The nature of the other boundaries of the Tumrok block has not been determined, as they are overlapped by a thick sequence of late Cenozoic volcanics. Faulting within the block is widespread, and essentially the TR is a number of fault-bounded blocks, probably on all scales. The best-preserved rock successions are composed (from base to top) of picritic–basaltic, tuff–sedimentary, basalt–andesitic and terrigeneous suites (Zinkevich *et al.*, 1991). The ultramafics occur within the thick (observed thickness ~1200 m) picrite–basaltic suite, mainly as

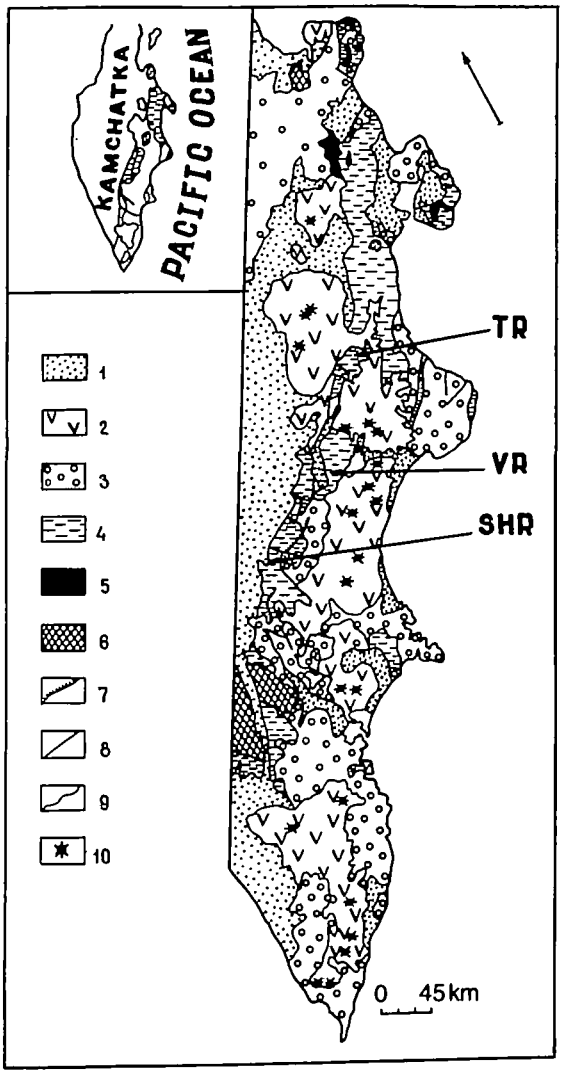

Fig. 1. Geological map of East Kamchatka (Zinkevich *et al.*, 1990). Arrow shows North. 1, Pliocene–Quaternary sediments; 2, Pliocene–Quaternary volcanic belt; 3, Cenozoic volcanics and sediments; 4, Late Cretaceous and Paleogene volcanic and sedimentary complexes including ultramafic volcanics; 5, peridotites; 6, metamorphic rocks; 7, tectonic nappes; 8, faults; 9, geological boundaries; 10, modern volcanoes. VR (Valaginsky Range), TR (Tumrok Range) and SHR (mountain Sharomsky Mis) refer to localities of ultramafic and basaltic rock samples.

pillow lavas and tuffs, but dykes and sills are also common. Picritic layers (3–5 m thick) are interbedded with basaltic pillow lavas, tuffs and breccias (5–30 m thick). The number of picrite flows increases toward the top of the picritic–basaltic suite, but overall they form less than 1% of this suite. Swarms of subparallel comagmatic picrite and basalt dykes and sills that range in thickness up to ~20 m cut the lavas and tuffs in all parts of the suite. The volcanics are associated spatially and possibly genetically with a large (5 km × 2 km) layered intrusive body, composed of apodunite serpentinites at the base, followed upward by olivine pyroxenites, troctolites, plagioclase pyroxenites, gabbros and syenites. Some outcrops show compositional layering with rhythmic distribution of rock types.

PETROGRAPHY AND MINERALOGY

The ultramafic volcanics of Eastern Kamchatka are strongly porphyritic picrites usually with a glassy to microcrystalline matrix. Euhedral olivine phenocrysts up to 3 cm across dominate the phenocryst assemblage, and form up to 40–75% of the rock. Subordinate clinopyroxene phenocrysts (<1·5 cm) are also present in TR and SHR picrites (20% of rock) but are scarce in picrites from VR. Cr-spinel is common in all picrites as inclusions in phenocrysts, and more rarely as discrete phenocrysts. The glassy matrix has a typical spinifex texture in TR and VR ultramafic lavas, and is composed mainly of altered glass, clinopyroxene and phlogopite, but K feldspar, plagioclase, apatite and amphibole are also present as groundmass phases in some rocks, especially in TR picrites. Titanomagnetite is common as groundmass grains in more crystalline matrix. All rocks show some degree of alteration. Secondary minerals such as serpentine after olivine, carbonate and chlorite after glass, and albite after plagioclase are fairly common. We focused this study on the least-altered rocks in our collection.

Phenocrystal olivine, clinopyroxene and Cr-spinel compositions, plus compositions of magmatic inclusions, were analysed by a Camebax electron microprobe in the Vernadsky Institute of Geochemistry, Moscow, using operating conditions at 30 nA current, 15 kV accelerating voltage and microprobe standards from the US Geological Survey (USGS) collection (Jarosewich *et al.*, 1980), and established Russian olivine (CH-1) and spinel (UV-126) standards (Lavrent'ev *et al.*, 1974).

Olivine

Olivine phenocryst compositions range from Fo_{86} to Fo_{95} but most samples have $Fo_{90–92}$ [Fig. 2a, Table 1, and data of Markovsky & Rotman (1981)]. They are typically unzoned, although rare crystals show some normal or reversed zoning. CaO contents of olivine phenocrysts vary from 0·01% to 0·55%, with low-Ca olivine being more common in VR picrites (up to 50% of samples studied—Fig. 2b). The wide range of CaO contents in olivine phenocrysts (Figs 2b and 3) suggests that they belong to several genetic populations. NiO concentrations of olivine phenocrysts range from 0·24% to 0·42% and from 0·14% to 0·37% in VR and TR ultramafic volcanics, respectively. Regional variation of NiO contents in olivine (Fig. 3) is noted and is related to whole-rock geochemistry (see Fig. 8a, below).

Cr-spinel

High-Cr, high-Mg spinel depleted in Ti and Al is ubiquitous in all studied ultramafic lavas and dykes [Fig. 4, Table 1, and data of Markovsky & Rotman (1981)]. The close compositional similarity in *cr*-number and *mg*-number values of these Cr-spinels to those from high-Mg island arc basalts (e.g. Sigurdsson *et al.*, 1993) is emphasized. The Cr-spinels are relatively oxidized and in this respect are comparable with those from the New Georgia picrites (Ramsay *et al.*, 1984), picrites from Ambae (Aoba) volcano (Eggins, 1993) and Siberian meimechites (Sobolev & Slutsky, 1984).

Cr-spinels from TR ultramafic lavas are slightly enriched in Al_2O_3 and depleted in TiO_2 compared

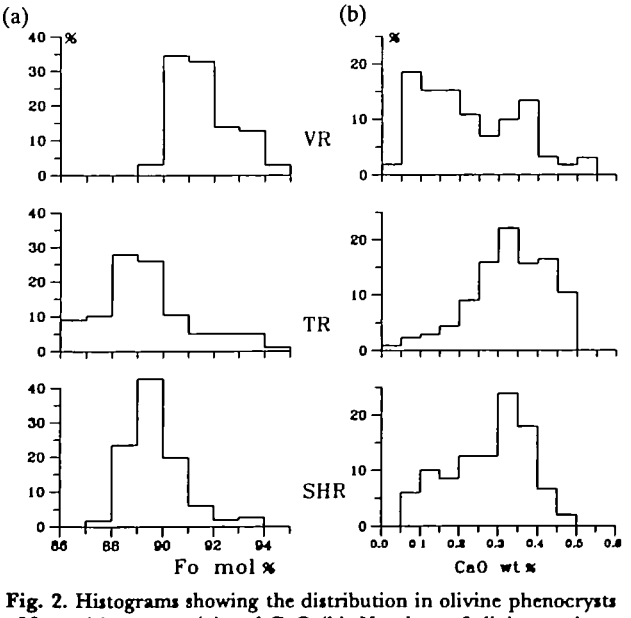

Fig. 2. Histograms showing the distribution in olivine phenocrysts of forsteritic content (a) and CaO (b). Numbers of olivine analyses for Fo and CaO are: VR—374 and 306; TR—219 and 335; SHR—103 and 151.

Table 1: Representative compositions of phenocrysts and their spinel inclusions

Region	TR	TR	TR	TR	TR	VR	VR
Sample	DAN-51	DAN-51	DAN-51	DAN-73	DAN-63	KB-74	KB-188
Olivine							
SiO_2	40·71	41·62	40·99	40·88	39·93	41·52	40·66
FeO	12·42	9·16	7·09	9·85	14·47	6·59	6·26
MnO	0·24	0·15	0·12	0·20	0·29	0·14	0·14
MgO	47·33	50·10	52·63	48·04	44·89	51·05	51·61
CaO	0·43	0·29	0·32	0·40	0·31	0·23	0·24
Cr_2O_3	0·03	0·08	0·12	0·09	0·04	0·12	0·07
NiO	0·15	0·15	0·22	0·20	0·15	0·31	0·35
Total	101·31	101·55	101·49	99·66	100·08	99·96	99·33
Fo*	87·17	90·70	92·97	89·69	84·69	93·25	93·63
Spinel							
SiO_2	0·11	0·11	0·14	0·13	0·13	0·10	0·19
TiO_2	0·89	0·29	0·32	0·44	0·71	0·39	0·18
Al_2O_3	8·81	8·70	8·69	8·73	9·80	7·66	5·62
Fe_2O_3†	28·74	10·70	12·72	14·72	29·74	17·43	9·75
FeO	18·04	13·70	10·37	15·51	23·28	12·97	10·83
MnO	0·31	0·25	0·22	0·27	0·28	0·23	0·24
MgO	10·26	12·69	15·20	11·72	7·03	13·09	14·18
Cr_2O_3	32·94	52·48	52·70	48·19	29·94	47·24	57·55
V_2O_3	0·14	0·08	0·05	0·05	0·13	0·06	0·03
Total	100·24	99·00	100·41	99·76	101·04	99·17	98·57
$Mg/(Mg+Fe^{2+})$*	50·35	62·28	72·32	57·40	35·00	64·28	70·01
$Cr/(Cr+Al)$*	71·50	80·18	80·27	78·74	67·21	80·53	87·29
Fe^{2+}/Fe^{3+}	0·70	1·42	0·91	1·17	0·87	0·83	1·23

with those in VR lavas, though there is a significant compositional overlap of the most primitive spinel compositions. On average, Fe^{2+}/Fe^{3+} values are also higher in TR spinel. The range in TiO_2 in high-Mg spinel is significant (0·2–1 wt %), overlapping at its lower end with primitive spinels from boninites and arc tholeiites (Sigurdsson *et al.*, 1993; Sobolev *et al.*, 1993; Sobolev & Danyushevsky, 1994) and high-K arc rocks (V. S. Kamenetsky, unpublished data, 1993) at its higher end. The trends of chemical evolution for TR and VR Cr-spinel inclusions in olivine and clinopyroxene are very similar (see Fig. 6) and provide evidence for continuous spinel crystallization during melt fractionation.

Clinopyroxene

Clinopyroxene phenocrysts are compositionally typical of arc basalt clinopyroxenes (Letterrier *et al.*, 1982), with high CaO and low TiO_2 contents and

Region	VR	VR	VR	VR		TR	VR
Sample	KB-64	KB-9	KB-194	KB-74		DAN-51	K-139
Olivine					*Clinopyroxene*		
SiO_2	40·32	41·32	41·23	41·24	SiO_2	51·75	49·02
FeO	10·78	8·29	9·25	6·50	TiO_2	0·16	0·61
MnO	0·21	0·15	0·20	0·14	Al_2O_3	2·32	5·22
MgO	47·92	49·91	50·41	50·40	FeO	4·29	7·65
CaO	0·37	0·30	0·40	0·10	MnO	0·09	0·20
Cr_2O_3	0·02	0·08	0·00	0·09	MgO	17·34	14·67
NiO	0·30	0·33	0·33	0·42	CaO	22·33	22·03
Total	99·92	100·38	101·82	98·89	Na_2O	0·21	0·30
Fo*	88·80	91·48	90·67	93·25	Cr_2O_3	0·76	0·11
					Total	99·25	99·81
					$Mg/(Mg+Fe^{2+})$*	87·81	77·37
Spinel							
SiO_2	0·04	0·11	0·12	0·22		0·12	0·38
TiO_2	0·82	0·52	0·46	0·45		1·53	4·71
Al_2O_3	8·22	7·51	7·80	10·29		8·94	9·75
Fe_2O_3†	29·76	18·47	22·16	13·87		33·68	50·92
FeO	17·08	12·34	15·22	10·93		19·68	25·52
MnO	0·29	0·23	0·24	0·16		0·29	0·21
MgO	10·97	13·71	11·75	14·67		9·65	6·11
Cr_2O_3	34·17	46·97	42·62	47·37		26·70	5·43
V_2O_3	0·05	0·02	0·03	0·04		0·15	0·41
Total	101·40	99·88	100·40	98·00		100·74	103·44
$Mg/(Mg+Fe^{2+})$*	53·38	66·45	57·92	70·53		46·64	29·92
$Cr/(Cr+Al)$*	73·61	80·75	78·57	75·54		66·71	27·20
Fe^{2+}/Fe^{3+}	0·64	0·74	0·76	0·88		0·53	0·45

*Mol %.
†Calculated on the basis of stoichiometry.

variable contents of Cr_2O_3 and Al_2O_3 (Fig. 5; see Table 6, below). Clinopyroxenes from all localities show a similar range of *mg*-numbers (68–92) but differences in average Ti content, reflecting regional variation of Ti concentration in parental melts. Crystals often show strong normal zoning, with *mg*-number strongly correlated with SiO_2, Cr_2O_3 (positive) and Al_2O_3, TiO_2 and Na_2O (negative) contents.

Phase relationships in the phenocrysts assemblage

Compositions of Cr-spinel inclusions in olivine and clinopyroxene, and olivine inclusions in clinopyroxene are strongly correlated (Fig. 6). For the latter, regression of 13 olivine–clinopyroxene pairs yields the relation Fo(mol %) = 0·78 $mg\text{-number}_{Cpx}$ (mol %) + 17·9 (r = 0·92). This relation probably

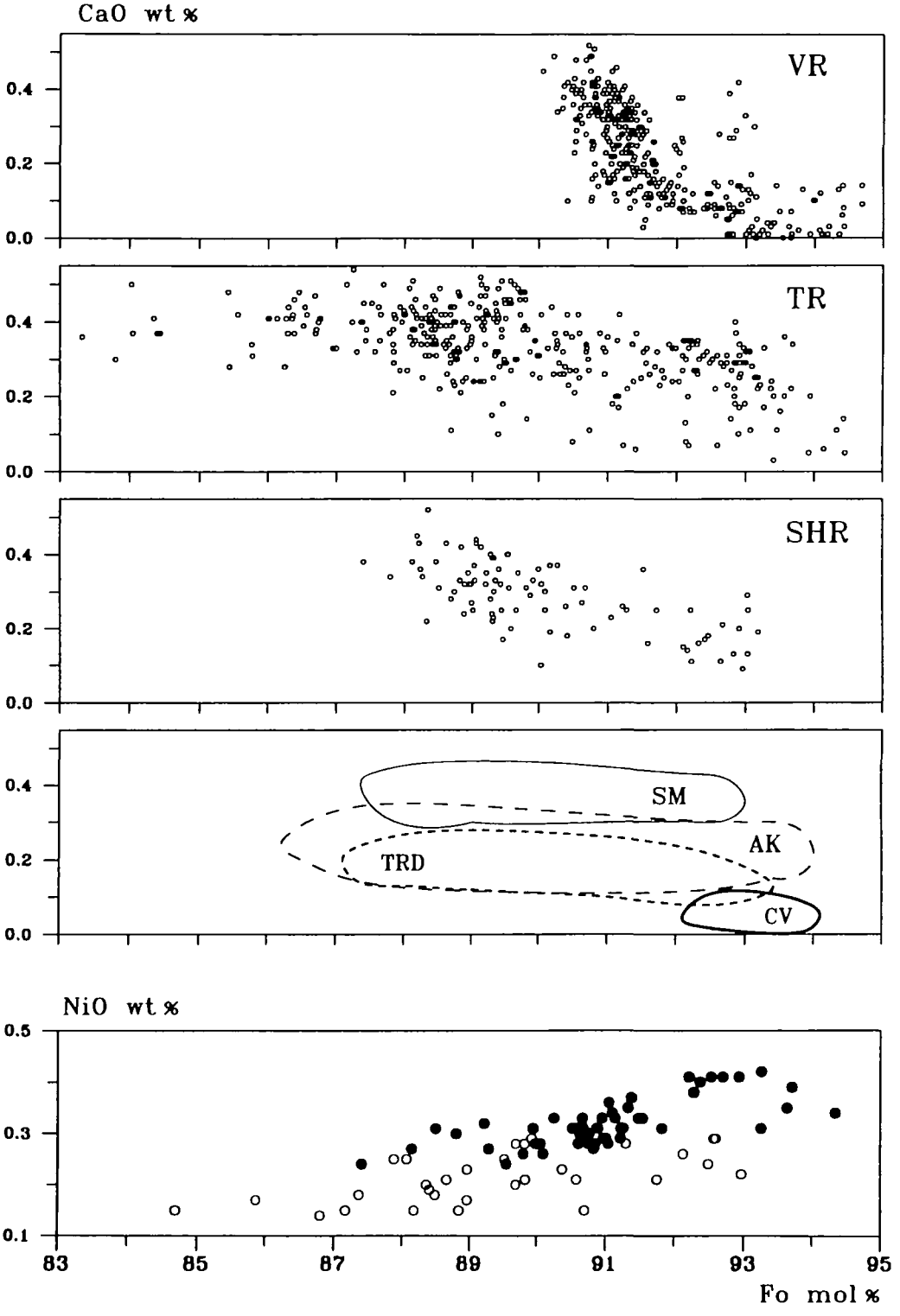

Fig. 3. Relationships between forsterite (Fo) and CaO or NiO content of olivine phenocrysts. SM—Siberian meimechites (Sobolev & Slutsky, 1984); AK—Archaean komatiites (Arndt & Nisbet, 1982; Arndt, 1986); TRD—Upper Pillow Lavas, Troodos, Cyprus (Sobolev *et al.*, 1993); CV—boninites from Cape Vogel, Papua New Guinea (Walker & Cameron, 1983; our unpublished data). On Fo vs NiO plot: ○, TR; ●, VR.

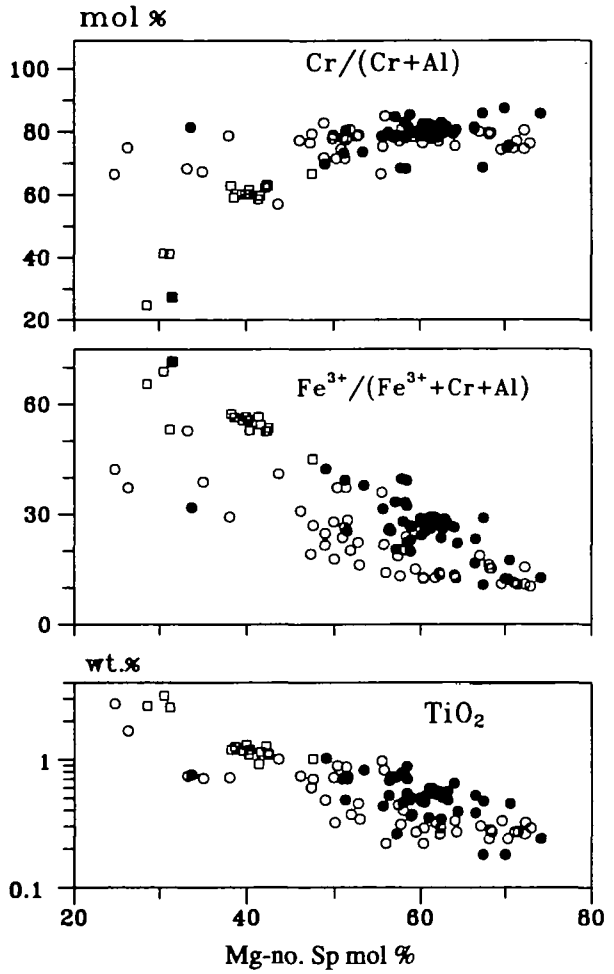

Fig. 4. The composition of chromium spinel inclusions in phenocrysts. Open symbols—TR; filled symbols—VR; circles—spinel in olivine; squares—spinel in clinopyroxene.

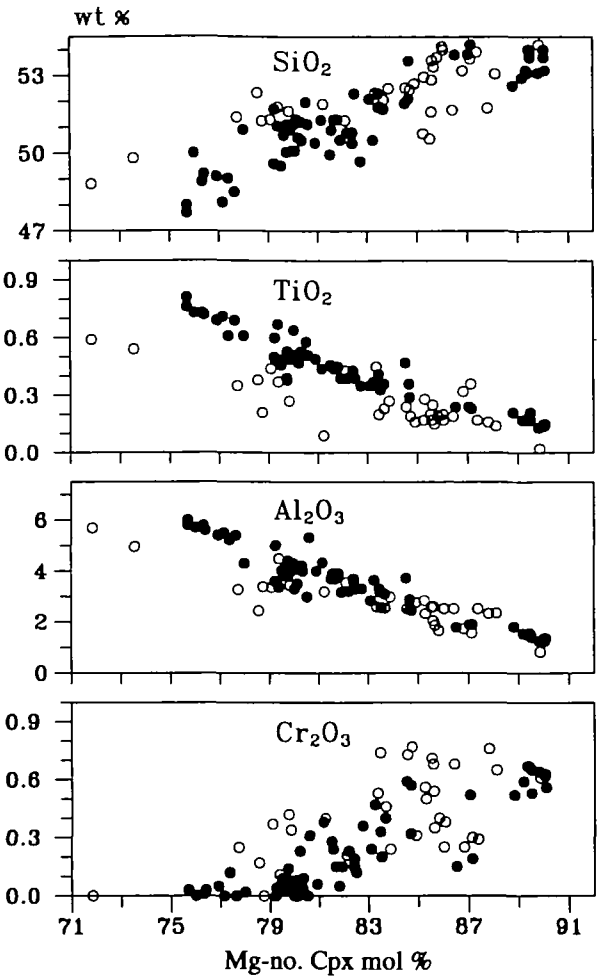

Fig. 5. The composition of clinopyroxene phenocrysts. *mg*-number = Mg/(Mg + Fe). Symbols as in Fig. 2.

reflects Ol–Cpx equilibrium during cotectic crystallization, and indicates insignificant Mg–Fe redistribution between these minerals at low temperatures, reflecting the weak temperature dependence of K_d(Mg,Fe) between Ol and Cpx (Duke, 1976). The *mg*-number (91–92) of the most magnesian clinopyroxene indicates that the beginning of clinopyroxene crystallization occurred at olivine compositions around $Fo_{89-89.5}$. The crystallization of Cr-spinel occurred from the very earliest stage of magma crystallization.

Inclusions in phenocrysts

Crystalline inclusions

Cr-spinel is the main crystalline inclusion in olivine. About 2% of VR olivines and 1% of TR olivines contain inclusions of low-Ca, low-Al pyroxene (Table 2, Nos 1–5). Oblique extinction, low birefringence and occasional polysynthetic twinning (Fig. 7) suggest that this phase is clinoenstatite (e.g. Dallwitz *et al.*, 1966). Excluding boninites, this is a unique occurrence of clinoenstatite in a terrestrial magmatic rock. Olivine hosting clinoenstatite inclusions is a high-Mg ($Fo_{>91.5}$), low-Ca (<0·2 wt % CaO) and high-Ni (>0·34 wt % NiO) composition, and a strong positive correlation exists between *mg*-number of clinoenstatite and Fo content of host olivine. The regression line is $mg\text{-number}_{Px}$ (mol %) = 0·95 Fo (mol %) + 5·97; r = 0·97 for five pairs. The clinoenstatite-bearing olivine phenocrysts also contain inclusions of silica-rich melt (Table 2, No. 5) as single inclusions with fluid bubbles, or in association with clinoenstatite.

Clinopyroxene phenocrysts contain olivine inclusions, and inclusions of high-Ca plagioclase (An = 93) are also present in some lower-Mg clinopyroxene grains (Table 2, No. 6).

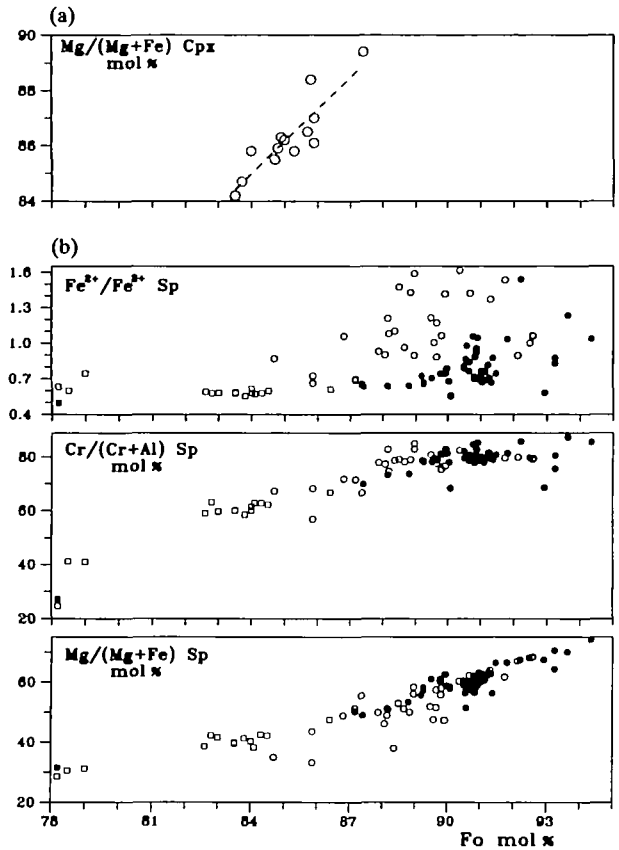

Fig. 6. Relationships between phenocryst compositions. (a) Compositional relationship between host clinopyroxene phenocrysts and olivine inclusions (for TR only). (b) Relationship between compositions of host olivine and clinopyroxene phenocrysts and spinel inclusions. Symbols as in Fig. 4.

Melt inclusions

Most melt inclusions in phenocrysts are glassy or partly crystallized. Tiny crystallites of clinopyroxene and an opaque phase are optically identified in inclusions in olivine. Pargasitic amphibole crystals are also optically identified in partly crystallized inclusions trapped in clinopyroxene (Table 2, Nos 7 and 8). The results of thermometric and microprobe study of melt inclusions are given below.

Xenocrysts

Rare grains of omphacite and high-Mg, high-Al orthopyroxene, the latter intergrown with low-Ca (CaO < 0·03%) olivine (Table 3), have been previously described from the VR ultramafic lavas (Sobolev *et al.*, 1990). Xenocrysts of Ca- and Cr-rich pyrope, low-Ca olivine and omphacite were also found in VR picrite tuffs (Seliverstov *et al.*, 1984). The extreme scarcity of xenocrysts and the limited available compositional data preclude further discussion of the implications of these findings.

GEOCHEMISTRY

Major elements

The strong negative correlation of MgO with Si, Al, Ca and Ti owing to crystallization and/or accumulation of olivine is shown by all the suites studied (Table 4, and Fig. 8a). The VR, TR and SHR ultramafic volcanics show a wide range of K_2O contents (0·1–2; 0·1–1·5 and 0·1–1%, respectively) that never correlates well with other major elements, including MgO. Loss on ignition (LOI) values are inversely correlated (Fig. 8b) with K_2O contents and Fe^{2+}/Fe^{3+}, suggesting that K_2O may have been leached from these glassy lavas with increasing extents of hydration. The ranges of CaO/Al_2O_3 values for least altered magmatic rocks are 0·5–2·1, 0·8–1·5 and 0·5–1·5 in VR, TR and SHR rocks, respectively. Some regional geochemical variations between the three suites are recognized. For example, the lowest contents of incompatible elements and Ni at a given MgO content are characteristic of TR picrites, whereas highest values occur in VR lavas, with SHR volcanics intermediate.

Trace elements

Trace elements in rocks were analysed by INAA at Laboratoire 'Pierre Süe' (CEN Saclay, France). Methods were described by Chayla *et al.* (1973). Trace element compositions of selected melt inclusions were analysed with an IMS-3F ion microprobe at the Massachusetts Institute of Technology, USA (Johnson, 1990). The results are reported in Tables 4 and 7 (below) and Fig. 9. As trace element patterns in the melt inclusions are very similar to whole-rock data, they are discussed together.

Three groups of incompatible elements, each showing different levels of concentration, may be distinguished. These are: (1) large ion lithophile elements (LILE—Cs, Rb, Ba, K and Sr), P and U; (2) rare earth elements (REE) and Th; (3) high field strength elements (HFSE—Ta, Nb, Hf, Zr and Ti).

LILE, P and U

These elements show a marked enrichment in comparison with other incompatible elements, typical of alkaline arc volcanics. However, for the LILE and U abundances in the rocks, the primary magmatic nature of this enrichment requires proof, as these rocks are strongly altered. The inverse correlation between K content and LOI (Fig. 8b) suggests that measured LILE abundances may be even lower than their initial concentrations. However, evaluation of trace element data for perfectly fresh melt inclusions (Fig. 9b) confirms unambiguously that the enrich-

Table 2: Compositions of magmatic inclusions (i) and host minerals (h)

	1		2		3		4	
Sample	KB-66		KB-32		KB-66		KB-66	
Phase	OL_h	PX_i	OL_h	PX_i	OL_h	PX_i	OL_h	PX_i
SiO_2	41·24	57·19	41·17	58·33	41·15	57·73	41·01	56·78
TiO_2	n.d.	0·08	n.d.	0·02	n.d.	0·01	n.d.	0·05
Al_2O_3	n.d.	0·28	n.d.	0·81	n.d.	0·27	n.d.	0·17
FeO*	6·33	4·46	6·46	4·29	8·27	5·54	7·76	4·91
MnO	0·09	0·12	0·08	0·11	0·13	0·24	0·14	0·11
MgO	50·89	36·15	51·56	36·01	49·43	33·49	49·05	33·72
CaO	0·09	0·71	0·10	0·81	0·21	1·64	0·10	0·20
Na_2O	n.d.	0·07	n d.	0·08	n.d.	0·07	n.d.	0·02
Cr_2O_3	0·07	0·29	n.d.	0·16	0·06	n.d.	0·06	0·09
NiO	0·41	n.d.	0·39	0·35	0·34	n.d.	0·40	n.d.
Total	99·12	99·35	99·76	100·97	99·59	98·99	98·52	96·05
mg-number	93·48	93·53	93·43	93·74	91·42	91·51	91·85	92·45

	5			6		7		8	
Sample	KB-9			K-139		K-139		TY-25	
Phase	OL_h	PX_i	GL_i	PX_h	PL_i	PX_h	AM_i	PX_h	AM_i
SiO_2	41·41	57·45	71·00	49·02	47·33	51·67	38·13	50·76	37·92
TiO_2	n.d.	0·02	0·47	0·61	n.d.	0·32	2·60	0·39	1·21
Al_2O_3	n.d.	0·18	17·05	5·22	31·17	3·09	14·99	3·88	17·95
FeO*	7·42	5·04	0·73	7·65	1·01	5·28	14·64	5·97	20·53
MnO	0·11	0·13	0·01	0·20	0·02	0·10	0·25	0·15	0·42
MgO	50·07	35·25	0·76	14·67	0·10	16·30	10·84	13·25	5·77
CaO	0·15	0·66	0·55	22·03	18·02	21·75	11·69	23·07	12·81
Na_2O	n.d.	0·05	2·03	0·30	1·41	0·22	2·17	0·21	2·21
K_2O	n.d.	n.d.	1·98	n.d.	0·14	n.d.	1·81	n.d.	0·97
P_2O_5	n.d.	n.d.	0·36	n.d.	n.d.	n.d.	0·65	n.d.	1·53
Cr_2O_3	0·05	0·17	n.d.	0·11	n.d.	0·54	n.d.	n.d.	n.d.
NiO	0·38	n.d.	n.d.	n.d.	n.d.	n.d.	n.d.	n.d.	n.d.
Total	99·59	98·95	94·94	99·81	99·20	99·27	97·77	97·68	101·32
mg-no.	92·33	92·58		77·37		84·62		79·83	
An					93·3				

1–4, pyroxene (clinoenstatite) inclusions in low-Ca olivine; 5, combined (clinoenstatite + glass + fluid) inclusion in olivine (see Fig. 7); 6, plagioclase inclusion in clinopyroxene; 7,8, combined (amphibole + glass + fluid) inclusions in clinopyroxene.
1–7, VR; 8, TR. *mg*-no., $Mg/(Mg + Fe^{2+})$ (mol %); An, anorthite component (mol %).
*Total iron as FeO.

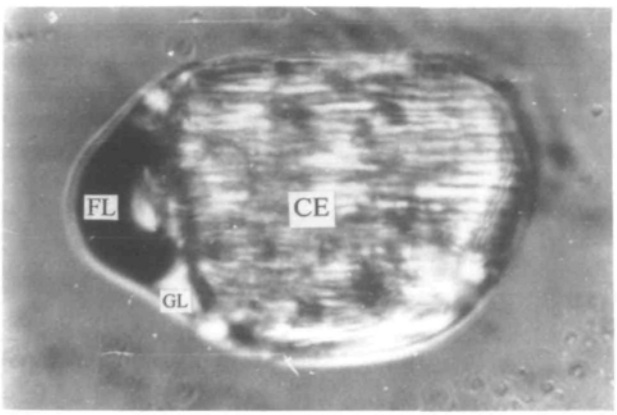

Fig. 7. Complex melt inclusion in low-calcium olivine consisting of clinoenstatite (CE), glass (GL) and fluid bubble (FL). See Table 2, No. 5. Inclusion size 35 μm.

ment is primary. This is also indicated by the good correlation between U and immobile Th.

REE and Th

These elements show intermediate levels of enrichment, and some regional variation. For example, VR and SHR picrites have a weak to moderate enrichment ($[Th/Sm]_n = 1{\cdot}4–2{\cdot}3$ and $1{\cdot}4–1{\cdot}7$, respectively), whereas TR melts are relatively depleted in Th and LREE ($[Th/Sm]_n = 0{\cdot}6–1{\cdot}0$). In contrast, HREE (Tb–Yb) contents are similarly depleted in all rocks.

High field strength elements (HFSE—Ta, Nb, Hf, Zr and Ti)

All studied ultramafic lavas and melts are depleted in these elements, particularly in Ta and Nb, with TR samples being the most depleted (Ta content is 10 times lower than estimates for the primitive mantle).

Nd–Sr isotopes

Fresh clinopyroxene phenocrysts were hand-picked, washed in HCl and analysed for Nd–Sr isotopes (Karpenko *et al.*, 1989) (Table 5). ε_{Nd} values of analysed samples lie in a narrow range of $+10{\cdot}7$ to $+9{\cdot}1$, and initial $^{87}Sr/^{86}Sr$ values vary from 0·70316 to 0·70358; the higher values may reflect limited seawater alteration. There are regional variations of isotopic signatures. The TR volcanics show the most depleted isotopic characteristics and also the most depleted incompatible element signatures (Fig. 9). Ultramafic lavas and basalts from the same area have similar isotopic signatures.

The parent magmas of this suite were clearly derived from a long-term depleted mid-ocean ridge basalt (MORB)-type source peridotite, but $^{87}Sr/^{86}Sr$ values are slightly shifted out of the mantle array toward higher $^{87}Sr/^{86}Sr$, a feature typical of many arc lavas (e.g. DePaolo & Johnson, 1979).

Table 3: Compositions of xenocrysts from VR ultramafic lavas

	1	2	3		4
Sample	KB-23	KB-10	KB-10	KB-10	KB-10
SiO_2	54·71	54·63	54·92	41·20	52·02
TiO_2	0·15	0·12	0·09	n.d.	0·43
Al_2O_3	4·64	4·08	3·41	n.d.	5·95
FeO*	6·54	6·31	6·45	9·86	2·14
MgO	32·83	33·83	33·18	47·57	15·05
CaO	0·65	0·43	0·41	0·03	20·54
Na_2O	0·13	0·06	0·04	n.d.	1·64
Cr_2O_3	0·28	0·27	0·25	n.d.	0·93
Total	99·93	99·73	98·75	98·66	98·70
mg-no. (mol%)	89·95	90·53	90·17	89·59	92·61

1,2, compositions of orthopyroxene; 3, compositions of orthopyroxene and olivine intergrowth; 4, composition of clinopyroxene. *mg*-no., $Mg/(Mg + Fe^{2+})$.
*Total iron as FeO.

Table 4: Representative major and trace element compositions of ultramafic volcanics from East Kamchatka

	Tumrok Range (TR)			Valaginsky Range (VR)			Sharomsky M. (SHR)		
Sample	DAN-51	DAN-67	Ty-25	KB-10	KB-74	K-139	SH-9	SH-18	SH-21
SiO_2	41·83	38·87	45·21	41·61	39·29	41·96	41·29	40·02	39·65
TiO_2	0·30	0·19	0·37	0·34	0·22	0·56	0·32	0·24	0·23
Al_2O_3	4·99	3·29	8·60	4·80	3·13	8·77	4·26	3·47	3·40
FeO*	9·98	9·36	9·87	8·99	8·33	9·49	9·11	8·95	9·00
MnO	0·22	0·21	0·17	0·17	0·17	0·17	0·15	0·15	0·15
MgO	25·65	33·31	20·19	30·05	36·33	16·36	28·89	32·31	32·96
CaO	7·11	3·55	7·66	6·00	3·61	9·52	5·62	3·44	3·58
Na_2O	0·31	0·05	0·52	0·29	0·10	0·73	0·13	0·08	0·07
K_2O	0·61	0·12	1·36	2·38	0·14	4·61	1·01	0·23	0·18
P_2O_5	0·17	0·10	0·22	0·22	0·17	0·32	0·21	0·12	0·12
Cr_2O_3	0·27	0·24	0·17	0·28	0·36	0·10	0·24	0·34	0·35
LOI	6·90	7·35	5·05	5·01	8·71	5·73	8·15	9·70	9·60
Total	98·34	96·64	99·39	100·14	100·56	98·22	99·38	99·05	99·29
La	0·82	0·705	0·91	5·25	2·04	6·02	3·11	1·77	1·95
Ce	3·48	3	2·73	11·3	5·6	15·7	7·05	6·28	6·12
Sm	0·689	0·473	0·908	1·95	1·09	3·07	1·63	0·944	0·942
Eu	0·29	0·18	0·335	0·52	0·31	0·808	0·48	0·3	0·28
Tb	0·134	0·091	0·197	0·225	0·118	0·38	0·171	0·11	0·12
Yb	0·66	0·41	0·96	0·76	0·44	1·14	0·59	0·5	0·5
Zr	13	n.d.	12	17	n.d.	60	23	12	n.d.
Hf	0·329	0·14	0·467	0·616	0·38	1·17	0·609	0·415	0·259
Ta	0·01	0·006	0·009	0·112	0·015	0·065	0·023	0·016	0·016
U	0·064	0·047	0·084	0·345	0·194	0·47	0·308	0·126	0·16
Th	0·103	0·117	0·103	0·79	0·419	0·63	0·538	0·258	0·27
Ba	50	57·3	196	455	106·3	3430	209	100	302
Sr	n.d.	n.d.	369	n.d.	n.d.	404	n.d.	n.d.	n.d.
Cs	1·27	0·17	2·04	1·08	0·13	2·14	0·84	0·4	0·23
Rb	37·8	3·9	63·5	82·3	4·7	207·2	33·6	8·1	8
Cr	1711	2479	1409	1803	2454	1435	1553	2183	2188
Co	94·4	110·2	73·7	86·7	97·9	68·9	91·4	98·9	100·2
Ni	661	955	639	1379	1711	672	1354	1557	1580
Sc	29·6	17·3	28·2	19·9	13·1	33·3	21·5	16·7	17

Trace element contents as p.p.m., oxides as wt %.
*Total iron as FeO.

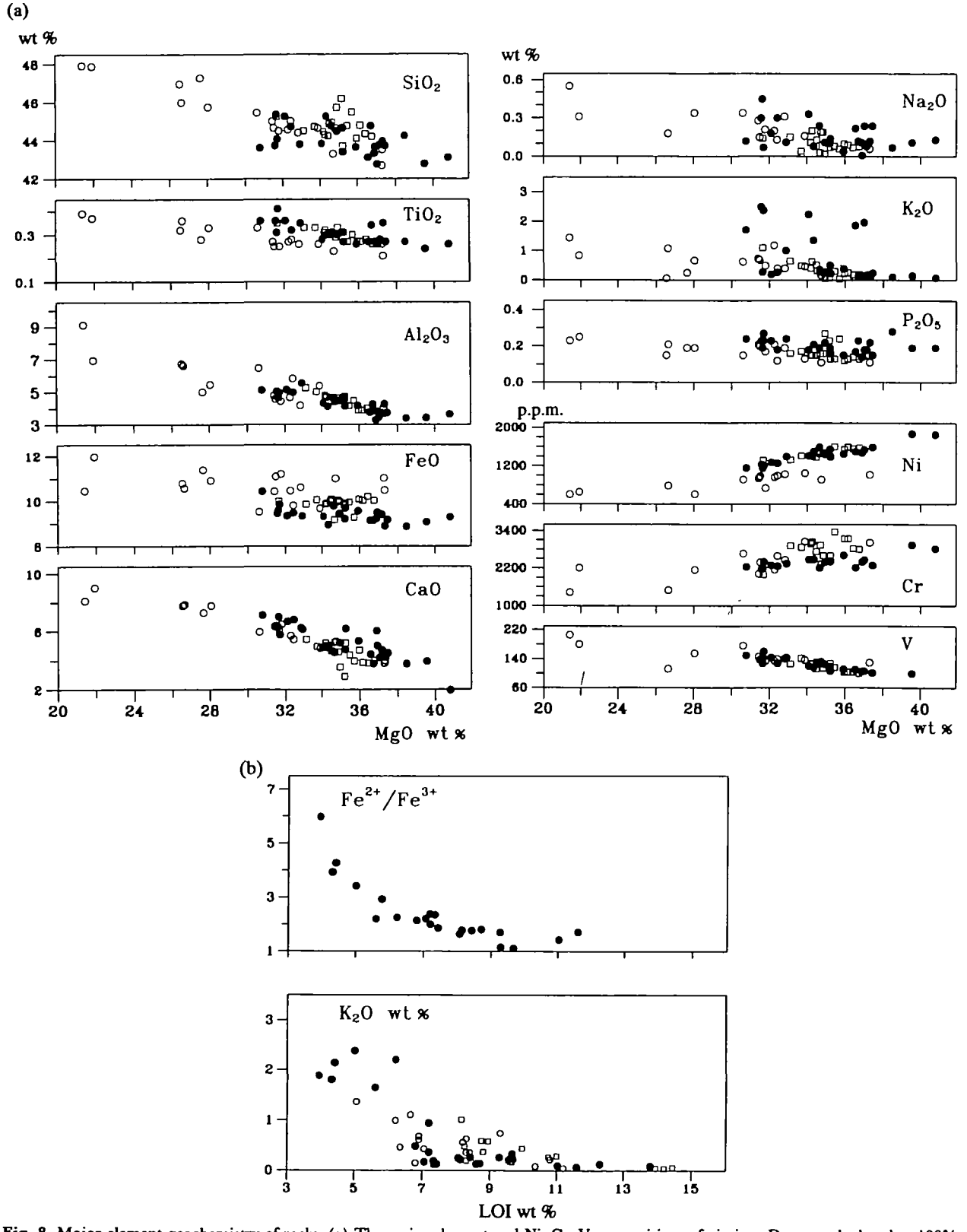

Fig. 8. Major element geochemistry of rocks. (a) The major element and Ni, Cr, V compositions of picrites. Data recalculated to 100% volatile-free. (b) Correlation between loss on ignition (LOI) and Fe^{2+}/Fe^{3+} and K_2O content in rocks. Fe_2O_3 was analysed only in VR rocks using 'wet' chemistry method. ○ TR; ●, VR; □, SHR.

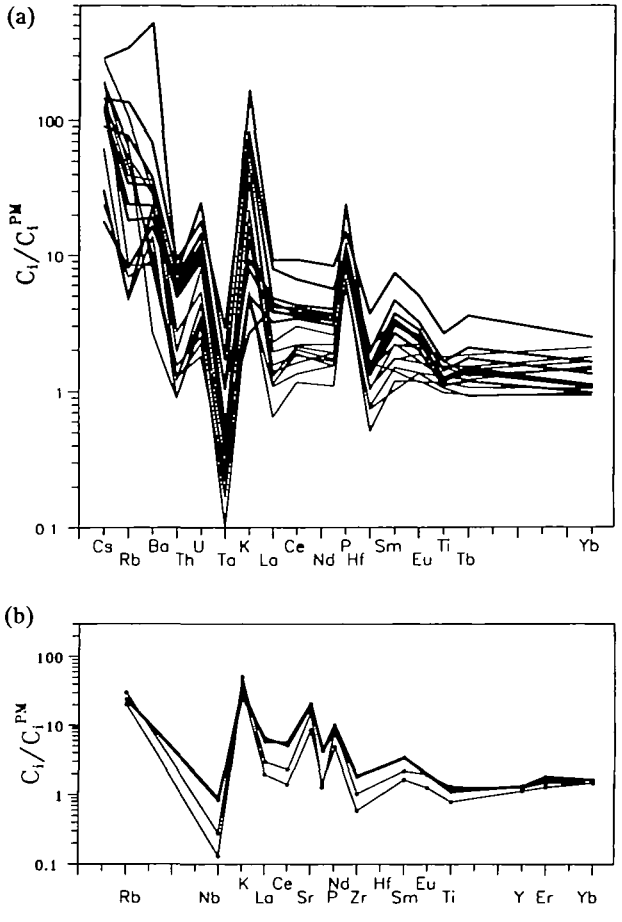

Fig. 9. Trace element composition of picrites (a) and melt inclusions (b). Thin lines—TR; bold lines—VR. Normalization is to primitive mantle (Sun & McDonough, 1989). To compare melt inclusions with rocks enriched in olivine, melt-inclusion data were renormalized to Yb content of rock host (Sample DAN-51 for TR) or typical (Sample KB-10 for VR). Data sources in Tables 4 and 7. (Note the close resemblance between whole-rock and melt-inclusion patterns.)

MELT-INCLUSION STUDY

Investigation of the melt inclusions in minerals is a useful technique for establishing crystallization conditions of the host volcanics (e.g. Roedder, 1984). For some cases in which rocks are strongly altered, this approach seems to be the only way to recover primary or near-primary conditions of magmas (e.g. Zlobin *et al.*, 1991). Details of the technique for the study and interpretation of melt inclusions in phenocrysts have been published elsewhere (e.g. Sobolev *et al.*, 1980, 1991, 1992; Roedder, 1984; Sobolev & Slutsky, 1984; Zlobin *et al.*, 1991; Danyushevsky *et al.*, 1992; Clocchiatti, 1993; Kamenetsky *et al.*, 1993; Sobolev & Danyushevsky, 1994).

High-temperature optical thermometry

A high-T experimental study of melt inclusions in olivine, clinopyroxene and Cr-spinel was carried out using the optical heating stage described by Sobolev *et al.* (1980), and an He atmosphere additionally purified with Zr powder at 800°C. Temperatures were measured with a $Pt–Pt_{90}Rh_{10}$ thermocouple and controlled by the melting point of gold in each run. The total measurement error in the device is estimated to be within ± 5°C. The f_{O_2} was controlled by a solid electrolyte cell and is close to the iron–wüstite buffer.

Systematic experiments with melt inclusions in olivine failed because of a high degree of grain cleavage, which leads to opening of the inclusion during the experiment. Successful melt-inclusion homogenization experiments ($T_h = 1270–1520$°C) described previously for these rocks (Sobolev *et al.*, 1990) do not show the expected correlation between host olivine composition and melt-inclusion homogenization temperature (T_{hom}). This may be due to olivine–melt re-equilibration at a late stage of crystallization, or alternatively, to decrepitation of inclusions.

On the basis of mineralogical data (Fig. 6a), the compositional range of olivine above an olivine–clinopyroxene cotectic has been established. Therefore, an alternative method to study melt inclusions is to heat the inclusions in high-Mg olivines (Fo > 90), which crystallized before clinopyroxene appeared, up to a reasonable temperature in the olivine-only field (e.g. $T = 1300$°C), with subsequent quenching. In this case, the composition of the melt in equilibrium with olivine at the measured temperature of quenching (T_q) may be determined, and thus the liquid composition in equilibrium with the most magnesian olivine may be established using thermodynamic modelling (see next section). This technique has been used for partly crystallized inclusions in sample KB-74 (VR).

Approximately 50 successful homogenization experiments were carried out with clinopyroxene grains from TR and VR picrites, picritic tuffs and basalts. The homogenization temperatures fall within 1030–1230°C and correlate well with the composition of host clinopyroxene (Kamenetsky *et al.*, 1993).

Melt inclusions hosted by spinel may preserve the initial melt compositions owing to absence of crystallization on the inclusion walls. About 60 grains of Cr-spinel from sample Ty-24 (TR) were heated to 1230–1380°C and quenched. Each grain was then mounted in epoxy, and gradually ground until melt inclusions were exposed on the surface. Quenched

Table 5: Sr and Nd isotopic composition of clinopyroxene phenocrysts from picrites and basalts

Sample	Region	Rock type	$^{87}Sr/^{86}Sr$	ε_{Nd}
DAN-44	TR	Basalt	0·70333	+10·3
DAN-51	TR	Picrite	0·70316	+10·7
SH-21	SHR	Picrite	0·70355	+9·1
K-139	VR	Picrite	0·70356	+9·7
KB-38	VR	Basaltic tuff	0·70345	+9·8
KB-180	VR	Picrite	0·70358	+9·2

Samples were hand-picked fresh clinopyroxene phenocrysts, leached using 0·1 N HCl (Karpenko *et al.*, 1989).

inclusions contain glass and very small (<1–2 μm) rounded daughter olivine crystals, which remained unmelted. The amount of this olivine cannot be estimated precisely on account of non-transparency of host spinel.

Melt-inclusion compositions

The compositions of all melt inclusions in olivine regardless of quenching temperature in the field of melt–olivine equilibrium differ from the true composition of trapped melt only either by crystallization of olivine on the walls of the inclusion in the case of underheating, or by remelting of olivine in the case of overheating. However, compositions of such inclusions offer useful information on the concentration and ratios of elements incompatible in olivine. The compositions of inclusions in Cr-spinel lie along the trend controlled by olivine, and melt MgO contents are underestimated, because only the glassy parts of inclusions were analysed, and crystals of unmelted olivine were not taken into account. The most Mg-rich compositions (Figs 10 and 11) are from experiments on olivine (VR) and Cr-spinel (TR) melt inclusions, whereas evolved melt compositions occur in the VR and TR clinopyroxene.

Compositions of TR melt inclusions fall along two trends: the 'olivine' trend for MgO > 8·5–9·0 wt %, and the 'olivine–pyroxene' trend (± titanomagnetite) for MgO < 8·5–9·0 wt % (Fig. 10 and Table 6). These trends correspond well to those derived from the whole-rock analyses for most elements, except alkalis (particularly, Na) and Ca for basalts.

A wide range of SiO_2, CaO, K_2O, P_2O_5 and FeO concentrations are observed (Fig. 11) in VR melt inclusions [and also by Sobolev *et al.* (1990)], and cannot be explained by olivine fractional crystallization. Distinct compositional diversity almost certainly exists among the primary melts of this region, and this diversity may exist even within inclusions in phenocrysts from a single lava sample.

Most melts from both localities, including high-Mg melt, are high-K ($K_2O > 1$ wt %). Three inclusions have notably lower K_2O and P_2O_5 contents.

The H_2O contents of melt inclusions (Table 8) were measured directly by an IMS-3F ion microprobe (CPRG, Nancy, France). Details of this analytical technique will be published elsewhere (Sobolev & Chaussidon, 1995). Calibration used standard basalt and high silica glass compositions covering a range of H_2O contents from 0·1–3·0 wt %. The H_2O measurement error is <20 relative %. Measured H_2O contents vary from 0·6 wt % for ultramafic melts to 1·2 wt % for basaltic melts. The Cl contents measured in melt inclusions in TR basalts using the electron microprobe are up to 0·4 wt % (Table 6).

PETROLOGY

The character and physico-chemical evolution of the magmatic system (primary melt composition, temperature, pressure and volatile contents) during crystallization may be established using results of our study of mineralogy and melt inclusions.

Primary melt

We define primary melt as the melt composition last in equilibrium with the source mantle at the time of melt segregation from that source. Compositions of primary melt were calculated using numerical modelling of reverse fractional crystallization of olivine. Starting compositions of the melt used in calcula-

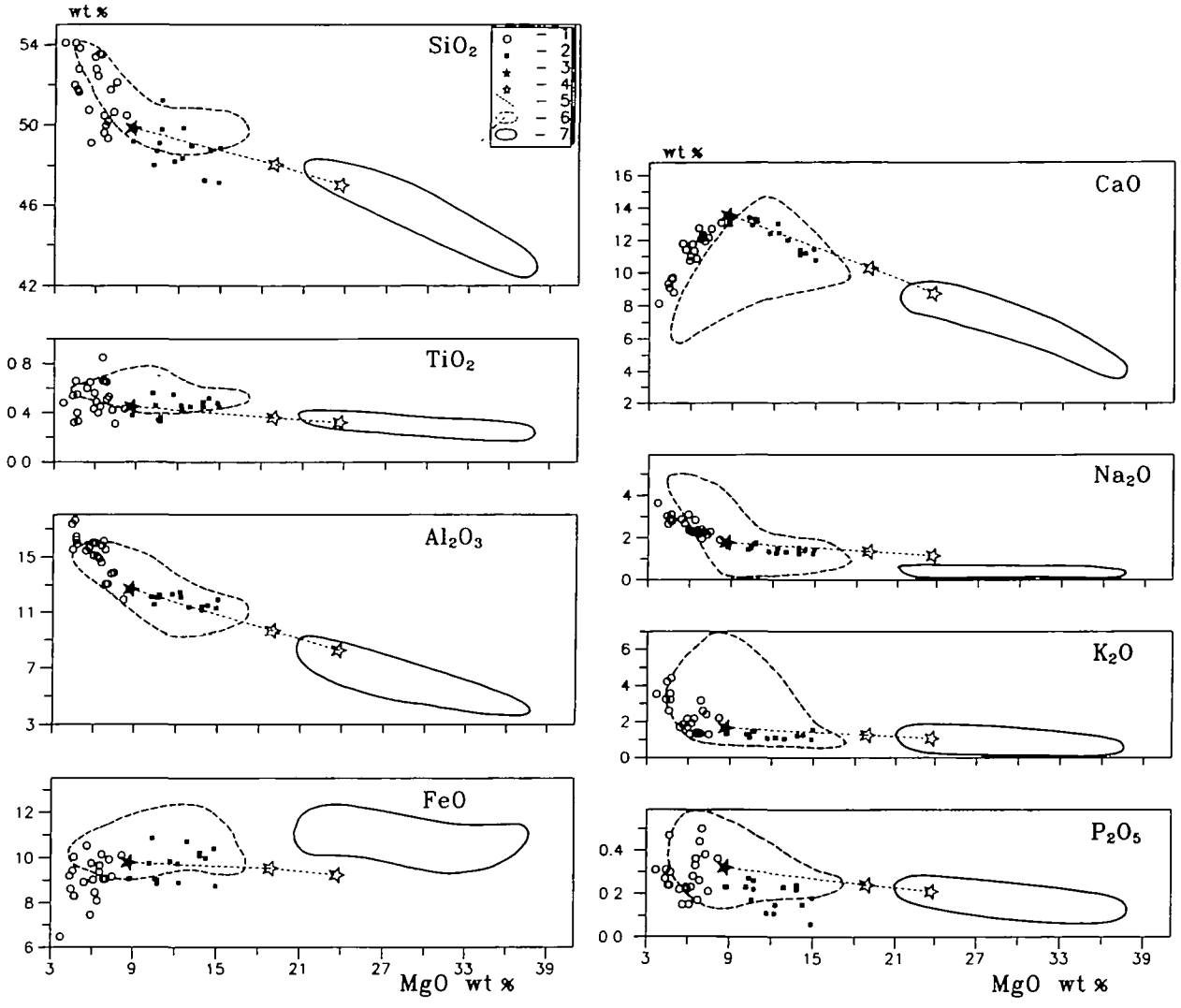

Fig. 10. Composition of melt inclusions in minerals from TR picrites and associated basalts compared with composition of rocks (picrites and basalts). 1—Homogenized melt inclusions in clinopyroxene; 2—melt inclusions in spinel; 3—calculated melt in the most magnesian clinopyroxene (Table 9, No. 1); 4—calculated primary melts (Table 9, Nos 2 and 3); 5—calculated trend of olivine fractionation; 6—basalts; 7—ultramafic volcanic rocks.

tions were taken from experimental data on the melt inclusions, notably, those in the most magnesian Cpx for TR and in olivine $Fo_{91\cdot2}$ for VR (Table 9). Two alternative models of olivine–melt equilibrium (Ford *et al.*, 1983; Sobolev & Slutsky, 1984) were used. The first model predicts nearly constant K_d (Fe–Mg) with changing temperature, giving values typical of accepted models (e.g. Roeder & Emslie, 1970). The second model was generated from a database of pre-1983 experimental studies of high-temperature (>1400°C) komatiitic-type melts, and predicts a significant positive correlation between K_d value and temperature. A recent evaluation of melt–olivine equilibria at $T>1300$°C (Sobolev & Danyushevsky, 1994) indicates that the Ford *et al.* and Sobolev & Slutsky models broadly define the lower and upper brackets, respectively, of all available data. Thus we use these models as lower and upper bounds of K_d estimations. Another three critical factors involved in this calculation include the composition of the primary liquidus assemblage, melt composition at any stage of crystallization within the olivine field, and the variation of melt Fe^{2+}/Fe^{3+} value.

The primary liquidus assemblage consists of high-Mg olivine and high-Cr spinel. Estimation of the composition of the most primitive olivine is problematic, owing to occurrence of olivine phenocryst groups with differing CaO contents. The most magnesian olivines of the high-Ca group (Fo_{93} and Fo_{94} for VR and TR, respectively, Fig. 3) were used

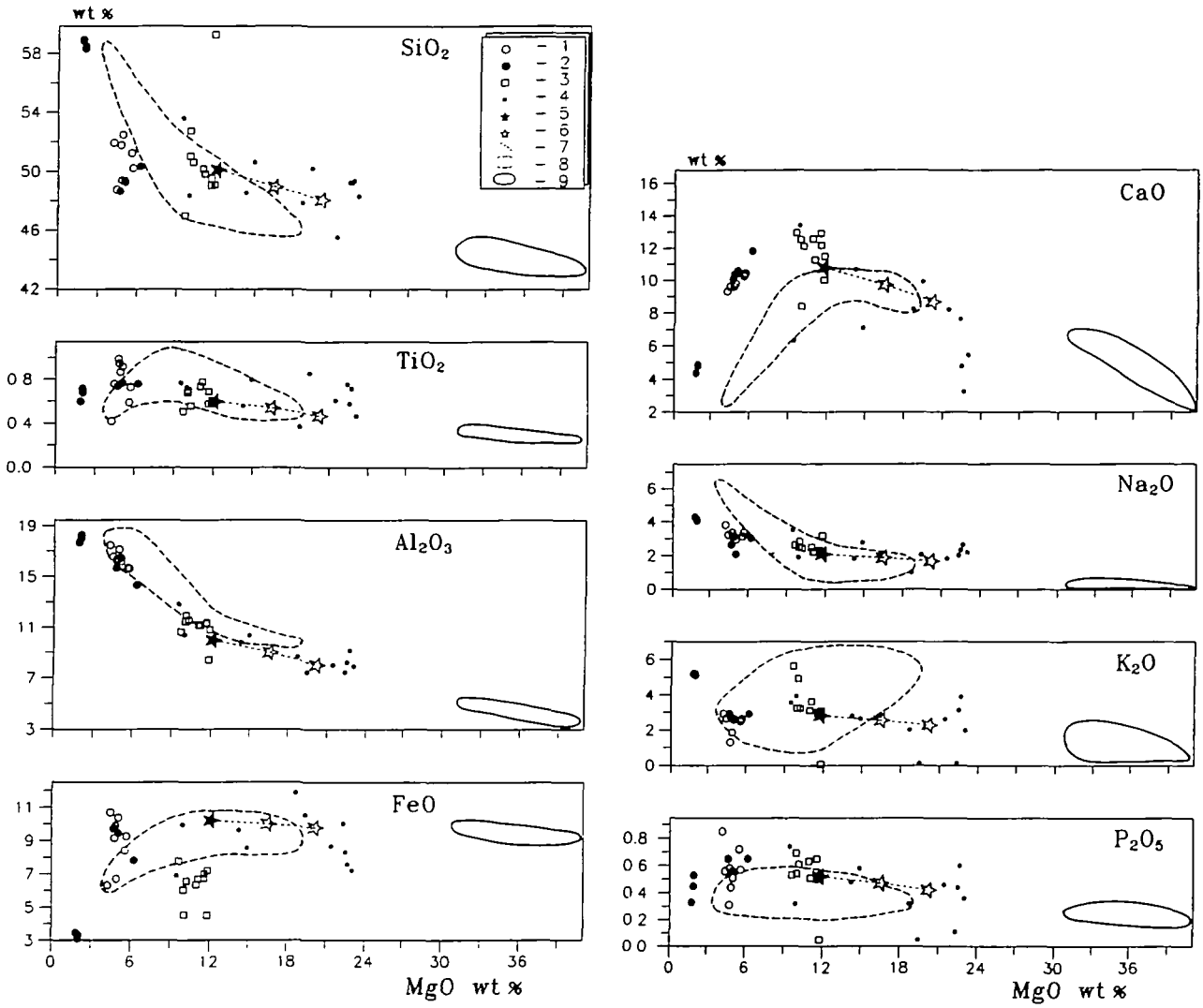

Fig. 11. Composition of melt inclusions in minerals from VR picrites and associated basalts compared with composition of rocks (picrites and basalts). 1—Homogenized melt inclusions in clinopyroxene; 2—glassy melt inclusions in clinopyroxene; 3—partly homogenized (quenched from 1290–1300°C) melt inclusions in olivine (Sample KB-74); 4—homogenized melt inclusions in olivine (Sobolev *et al.*, 1990); 5—calculated melt in olivine Fo 91·2 mol % (Table 9, No. 3); 6—calculated primary melts (Table 9, Nos 4 and 5); 7—calculated trend of olivine fractionation; 8—basalts; 9—ultramafic volcanic rocks.

in these calculations, as these seem more appropriate for these high Ca/Al melt inclusion compositions. The melt composition in the olivine field was calculated for TR and VR as follows:

(1) a melt in equilibrium with the most magnesian clinopyroxene phenocryst was used for TR. This composition (Table 9, No. 1) was chosen on the basis of experiments with melt inclusions in clinopyroxene and Cr-spinel (Fig. 10). The calculated melt composition reflects that stage of magma evolution at which the melt achieved its highest CaO content, marking the start of clinopyroxene crystallization.

(2) The composition of melt inclusions quenched at $T = 1300°C$ in olivine $Fo_{91·2}$ (Table 6, No. 13) corrected for FeO (Table 9, No. 4) was used for VR. This correction is necessary because FeO content (6·65 ± 0·36 wt %) in melt inclusions in KB-74 olivine is lower than in the whole-rock analysis (9·07 wt % after recalculation to 100%). Therefore, we used the FeO content of the groundmass of this sample (10·28 wt %), calculated by subtraction of 73% (optical point counting) of average olivine $Fo_{91·2}$ from whole-rock composition. We then confirmed from K_d relationships that this calculated groundmass composition is in equilibrium with the most evolved olivine Fo_{90} in the sample.

Table 6: Compositions of melt inclusions in clinopyroxene (1–12) and olivine (13)

	1	2	3	4	5	6	7	8
Sample	Ty-17	Ty-7	Ty-1	Ty-14	Ty-14	Ty-21	DAN-51	DAN-51
Melt								
SiO_2	52·00	54·09	52·44	53·51	53·55	50·47	49·34	50·48
TiO_2	0·54	0·32	0·49	0·45	0·40	0·85	0·51	0·43
Al_2O_3	17·34	15·53	15·98	14·89	15·05	14·60	13·04	11·91
FeO*	9·20	8·62	9·02	8·09	8·46	9·37	9·05	10·09
MnO	0·16	0·20	0·19	0·17	0·19	0·23	0·21	0·20
MgO	4·38	4·46	6·10	6·38	6·22	6·55	6·86	8·18
CaO	9·35	9·10	11·76	10·88	11·36	12·74	12·17	13·09
Na_2O	3·02	2·65	2·32	2·83	2·25	2·34	1·95	1·90
K_2O	3·24	4·21	1·31	2·16	1·90	1·37	3·16	2·18
P_2O_5	0·27	0·31	0·15	0·28	0·23	0·33	0·44	0·36
Total	99·50	99·49	99·76	99·64	99·61	98·85	96·73	98·82
Host mineral								
SiO_2	50·22	51·31	51·27	52·68	53·71	54·12	52·83	51·75
TiO_2	0·43	0·28	0·43	0·16	0·19	0·20	0·17	0·16
Al_2O_3	4·56	3·33	3·54	2·76	1·66	2·52	2·04	2·33
FeO*	7·98	7·47	6·05	5·18	4·94	4·98	4·83	4·29
MnO	n.d.	n.d.	n.d.	n.d.	n.d.	0·10	n.d.	0·09
MgO	14·15	15·06	15·60	16·33	16·76	17·10	16·10	17·34
CaO	22·01	22·04	22·60	22·24	22·32	22·16	22·69	22·32
Na_2O	0·34	0·25	0·21	0·31	0·40	0·16	0·17	0·21
Cr_2O_3	n.d.	n.d.	n.d.	n.d.	n.d.	0·25	0·54	0·76
Total	99·69	99·74	99·70	99·66	99·98	101·57	99·37	99·25
mg-no.	75·97	78·23	82·13	84·90	85·81	86·01	85·60	87·81
T_{hom} (°C)	1110	1105	1125	1135	1140	1165	1170	1175

(3) The degree of Fe oxidation in the melt was calculated using Fe^{2+}/Fe^{3+} of Cr-spinel and the empirical model of Maurel & Maurel (1982) as well as a relationship between $(Fe^{2+}/Fe^{3+})_{Sp}$ and equilibrium olivine (Fig. 6b). The regression line for VR is $(Fe^{2+}/Fe^{3+})_L = 0{\cdot}31 \times Fo - 26$, $R = 0{\cdot}66$ for 35 pairs. No significant correlation between these parameters was observed for TR samples (Fig. 6b), thus a mean value $(Fe^{2+}/Fe^{3+})_L = 3$ was used.

The primary melt compositions of Kamchatka ultramafics calculated on the basis of both limiting models of olivine–anhydrous melt equilibrium are given in Table 9. The MgO range of these calculated primary melts is 16·6–20·3 wt% (VR) and 19·0–23·8 wt% (TR). The primary melt composition calculated for VR ultramafics is close to that estimated from whole-rock chemistry (Sobolev *et al.*, 1990), with 21·7–23·5 wt% MgO for equilibrium with olivine $Fo_{93·5}$.

Assuming that the models used are correct, the error in final primary melt composition comes mostly from the uncertainty in FeO estimation of starting melt composition, and from the uncertainty

Table 6: continued

	9	10	11	12		13	σ
Sample	K-139	K-139	KB-38	KB-38		KB-74	
Melt							
SiO_2	50·22	51·24	49·40	48·77		49·91	0·69
TiO_2	0·73	0·59	0·95	0·76		0·66	0·08
Al_2O_3	15·64	15·68	16·36	16·59		11·27	0·23
FeO*	9·25	8·40	9·87	10·70		6·65	0·36
MnO	0·20	0·17	0·22	0·22		0·11	0·02
MgO	5·68	5·58	4·83	4·46		11·06	0·66
CaO	10·43	10·26	10·35	9·61		12·15	0·55
Na_2O	3·36	3·13	3·13	3·23		2·34	0·12
K_2O	2·62	2·49	2·71	2·66		3·18	0·21
P_2O_5	0·57	0·72	0·58	0·56		0·59	0·07
Total	98·70	98·26	98·40	97·56		97·92	
Host mineral							
SiO_2	50·52	49·96	51·28	50·04		41·32	0·25
TiO_2	0·37	0·46	0·44	0·39		n.d.	n.d.
Al_2O_3	3·64	3·70	4·33	4·25		n.d.	n.d.
FeO*	5·76	6·40	6·42	6·97		8·57	0·18
MnO	0·09	0·12	0·16	0·15		0·17	0·02
MgO	16·04	15·84	15·51	15·38		49·70	0·36
CaO	21·99	22·03	22·29	21·98		0·54	0·03
Na_2O	0·29	0·29	0·27	0·24	NiO	0·31	0·03
Cr_2O_3	0·47	0·28	0·38	0·14		0·05	0·01
Total	99·17	99·08	101·08	99·54		100·66	
mg-no.	83·24	81·52	81·16	79·73		91·18	
T_{hom} (°C)	1135	1130	1095	1070	T_q (°C)	1290–1300	

1–12, homogenized inclusions in clinopyroxene (1–8, TR; 9–12, VR); 13, average ($n=7$) composition of melt inclusions in olivine (Sample KB-74; see text) quenched from $T=1290$–1300°C; σ, standard deviation. 1–5 were analysed on Camscan Link System (Moscow State University). Cl content (wt%) in melt inclusions is: 0·38 (No. 2), 0·21 (No. 3), 0·31 (No. 4)—data from Camebax microbeam. *mg*-number is in mol. %; T_{hom}, temperature of homogenization; T_q, temperature of quenching.
*Total iron as FeO.
Ty-17, Ty-7, Ty-1, Ty-14, Ty-21 and KB-38 are basalts; DAN-51, K-139 and KB-74 are picrites.

in Fe^{2+}/Fe^{3+} of spinels. For example, the uncertainty in the degree of Fe oxidation may introduce an error of 6 relative % in the calculation of primary melt composition, which is well within the range produced using alternative models of olivine–melt equilibrium.

Crystallization conditions

Liquidus assemblage

The crystallization sequence for these magmas was liquidus olivine and Cr-spinel, followed by clinopyroxene and plagioclase, with gradual replacement of

Table 7: Trace element compositions of melt inclusions in phenocrysts

	1	2	3	4	5
Region	TR	TR	VR	VR	VR
Sample	DAN-51	DAN-51	KB-10	KB-38	KB-38
La	2·64	2·49	9·14	11·34	14·28
Ce	4·87	4·99	22·89	28·71	28·77
Nd	3·78	3·37	16·97	18·14	19·30
Sm	1·43	1·14	4·38	4·24	4·79
Eu	0·42	0·40	n.d.	n.d.	n.d.
Dy	1·86	1·44	2·88	3·78	3·81
Er	1·21	0·87	1·24	2·43	2·48
Yb	1·41	0·87	1·59	2·27	2·54
Rb	26·4	23·5	45·1	43·5	49·2
Sr	352	391	964	1258	1298
Nb	0·18	0·24	n.d.	1·7	2
Zr	13	14	55	57	65
Hf	n.d.	n.d.	n.d.	1·39	1·66
Tl	2033	2060	n.d.	4299	4604
Y	10	7	18	17	19
Cr	1509	726	461	53	41
SiO_2	46·57	44·23	48·36	49·38	48·67
TiO_2	0·30	0·29	0·47	0·77	0·74
Al_2O_3	9·60	6·36	7·94	16·48	15·68
FeO	7·89	11·42	7·21	9·44	9·72
MnO	0·12	0·21	0·16	0·16	0·17
MgO	20·82	22·96	23·03	5·06	4·70
CaO	8·65	9·65	5·47	10·44	10·07
Na_2O	1·38	0·88	2·19	2·09	2·64
K_2O	2·07	1·86	1·97	2·58	2·93
P_2O_5	0·21	0·23	0·36	0·56	0·65
Total	97·61	98·09	97·16	96·96	95·95

1–3, inclusions in olivine from picrites; 4 and 5, inclusions in clinopyroxene from basalt. Trace element contents as p.p.m., oxides as wt%.

Table 8: The compositions of melt inclusions in phenocrysts with measured H_2O contents

Region	TR	TR	VR	VR
Sample	DAN-51	DAN-51	KB-74	KB-194
Host	Ol	Cpx	Ol	Ol
SiO_2	44·23	50·48	49·83	49·27
TiO_2	0·29	0·43	0·78	0·58
Al_2O_3	6·36	11·91	11·15	8·25
FeO*	11·42	10·09	6·69	8·31
MnO	0·21	0·20	0·10	0·11
MgO	22·96	8·18	11·11	22·52
CaO	9·65	13·09	11·27	4·79
Na_2O	0·88	1·90	2·22	2·33
K_2O	1·86	2·18	3·62	3·13
P_2O_5	0·23	0·36	0·51	0·44
H_2O	0·63	0·61	1·23	0·61
Total	98·72	99·43	98·51	100·34

Major elements were measured by electron microprobe; H_2O by ion microprobe.
*Total iron as FeO.

Cr-rich spinel by titanomagnetite as crystallization proceeded. Although relatively high-Ca, high-Mg olivine was probably the major liquidus phase of the Kamchatka lavas, a melt with low-Ca olivine and clinoenstatite as a near-liquidus assemblage was also present at some early stage of crystallization.

Temperature

Crystallization temperatures in the basaltic compositional field were estimated via homogenization of melt inclusions in clinopyroxene. The positive correlation between clinopyroxene chemistry and T_{hom} (Sobolev *et al.*, 1990; Kamenetsky *et al.*, 1993) supports the fractional crystallization model and suggests that the temperature range of clinopyroxene crystallization was 1230–1030°C.

The temperature of olivine crystallization was calculated using the Ford *et al.* (1983) model at 1 atm. A correction for 1 wt % of H_2O (30°C) in the melt was taken into account (Danyushevsky *et al.*, 1992). Olivine crystallization started at 1400–1460°C in TR and 1380–1410°C in VR magmas (Table 9). The calculated and measured temperature range of olivine and clinopyroxene crystallization (1460–1030°C) demonstrates a very wide interval of cooling and crystallization of this ultramafic magma, during which the melt composition evolved from a P- and alkali-enriched picrite to a shoshonitic high-K basalt andesite (Figs 10 and 11) (Gill & Whelan, 1989).

Pressure

The low density determined for fluid inclusions in olivine and cpx phenocrysts (Sobolev *et al.*, 1990) is indicative of low-pressure phenocryst crystallization. The fluid pressure of crystallization estimated using the Burnham (1975) model is ~100 bar, with due regard for H_2O content in the melt (~1 wt %).

Volatiles

The Cl concentrations measured in melt inclusions (0·2–0·4 wt %) are well above those of MORB glasses (0·001–0·014 wt %) (Byers *et al.*, 1986), within-plate basalts (0·07–0·17 wt %) (Byers *et al.*, 1985) and high-Ca boninites (0·07–0·12 wt %) (Falloon & Green, 1986). Although similar high Cl concentrations are known in evolved basaltic glasses from the Galapagos spreading centre (up to 0·37 wt %) (Byers *et al.*, 1983, 1984) and high-K hawaiites from Etna (Metrich & Clocchiatti, 1989),

Table 9: Estimation of compositions, crystallization temperatures and pressure and temperature of generation of primary melts

	Tumrok Range (TR)			Valaginsky Range (VR)		
	1	2	3	4	5	6
SiO_2	50·41	48·02	46·99	50·14	48·95	48·10
TiO_2	0·45	0·34	0·29	0·60	0·54	0·47
Al_2O_3	12·82	9·67	8·20	10·20	9·00	8·03
Fe_2O_3		2·64	2·56		2·89	2·83
FeO	9·90*	7·14	6·92	10·28*	7·38	7·22
MnO	0·19	0·14	0·12	0·10	0·09	0·08
MgO	8·84	18·94	23·80	12·16	16·58	20·26
CaO	13·62	10·27	8·71	11·00	9·70	8·66
Na_2O	1·79	1·35	1·15	2·11	1·86	1·66
K_2O	1·66	1·25	1·06	2·88	2·54	2·27
P_2O_5	0·32	0·24	0·20	0·53	0·47	0·42
Fo (mol%)	89·1†	94·0‡		91·2†	93·0‡	
T (°C)		1400	1460		1380	1410
P (kbar)		40	50		32	40
T_L(°C)		1600	1710		1540	1610
T_A (°C)		1520	1610		1470	1530

1, calculated composition of melt in the most magnesian clinopyroxene; 4, calculated composition of melt in equilibrium with olivine Fo 91·2 mol%; 2,5 and 3,6, composition of primary melts calculated using models by Ford *et al.* (1983) and Sobolev & Slutsky (1984), respectively (see text). T, calculated temperature of melt in 'dry' equilibrium with olivine under 1 bar pressure minus 30°C (taking into account the presence of 1 wt% of H_2O). P, estimated pressure of last equilibrium of primary melts with Ol–Opx-bearing assemblage (see Fig. 12), T_L and T_A, estimated temperatures of this equilibrium, calculated using olivine liquidus slope as 5°C/kbar (Takahashi & Kushiro, 1983) and adiabatic slope as 3°C/kbar (Nisbet, 1982), respectively.
*Total iron as FeO.
†Composition of olivine in equilibrium with melt using $K_d = 0·31$.
‡The most magnesian high-Ca olivine.

the measured Cl concentrations in Kamchatka high-K melts are significantly higher than for any known primitive magmas.

The H_2O concentrations in Kamchatka ultramafic melts are lower than those of boninites and arc tholeiites (Danyushevsky *et al.*, 1993). The Kamchatka ultramafic melts are also distinguished from other mantle-derived magmas by their very high K_2O/H_2O values (>3).

P–T conditions of origin

The calculated primary melt compositions and their conditions of crystallization were used to estimate the *P–T* conditions of their last equilibrium with source peridotite. In this case, the uncertainties and errors in primary melt composition and its temperature will have a 'propagating' effect.

Pressure

Pressure was estimated on the basis of experimental data for peridotite partial melting under various *P–T* conditions. A projection from Cpx onto the plane Ol–SiO_2–Plag (Fig. 12) shows isobars calibrated from available published experimental data on liquids coexisting with lherzolite or harzburgite. The pressures obtained for segregation of VR and TR primary melts (Fig. 12) are 32–40 kbar and 40–50 kbar, respectively. Taking into account the influence

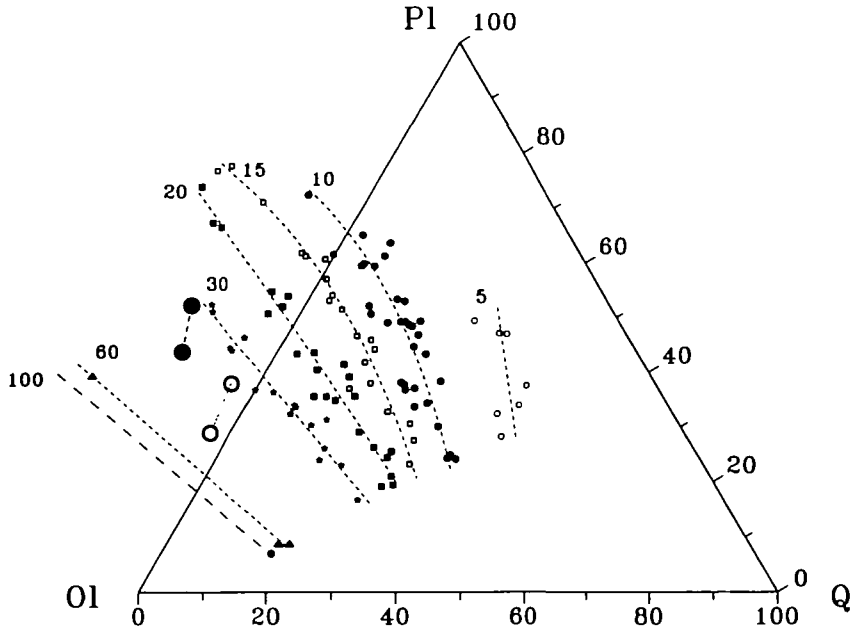

Fig. 12. Estimation of pressure of last equilibrium of primary melts with Ol–Opx-bearing assemblage. Projection of basaltic tetrahedron from Cpx apex (Takahashi & Kushiro, 1983). Isobars for melt composition calculated as linear (5, 20, 30 and 60 kbar) and polynomial (10 and 15 kbar) regressions of experimental data from Wendlandt & Eggler (1977); Takahashi & Kushiro (1983); Takahashi & Scarfe (1985); Takahashi (1986); Falloon & Green (1987, 1988); Falloon *et al.* (1988); Hirose & Kushiro (1993). ○, TR; ●, VR.

of high K_2O content on pressure estimations (Takahashi & Kushiro, 1983), these pressure estimates must be considered as lower limits. The occurrence of mantle garnet in VR ultramafic lavas (Seliverstov *et al.*, 1984) offers independent evidence for their high-pressure origin.

Temperature

The influence of H_2O (between 0·5 and 1·0 wt %) was taken into account in temperature calculations, using the method of Danyushevsky *et al.* (1992). The pressure influence on the temperature of melt generation was checked by two methods: (1) using the slope of liquidus curves for Ol-bearing systems, ~5°C/kbar (Takahashi & Kushiro, 1983), and (2) assuming adiabatic decompression of primary melt, with an adiabatic slope ~3°C/kbar (Nisbet, 1982). The calculated temperatures of primary melt generation for VR and TR lie in the interval of 1470–1610°C and 1520–1710°C, respectively (Table 9). Thus the Kamchatka ultramafic volcanics are another established example of high-T ultramafic magmatism of Phanerozoic age.

GEOCHEMICAL CLASSIFICATION

Kamchatka ultramafic volcanics were considered in the Russian literature to belong to the komatiite series (Markovsky & Rotman, 1981; Landa *et al.*, 1983) in terms of their high MgO content. However, an extension of the komatiite terminology (Arndt & Nisbet, 1982) and its implications to Cretaceous volcanics may not be very constructive. The basaltic members of the Kamchatka suite are similar in many respects to high-K arc shoshonites (high K/Na), and the entire suite shows both geological (e.g. Zinkevich *et al.*, 1989, 1991) and geochemical evidence for an island-arc origin. The latter include low HFSE contents in comparison with REE, high and variable levels of LILE enrichment in comparison with REE (e.g. Perfit *et al.*, 1980), high H_2O concentration in melts (e.g. Danyushevsky *et al.*, 1993; Sobolev & Chaussidon, 1995), and tendency towards more radiogenic Sr relative to the mantle array (eg. McCulloch & Gamble, 1991, and references therein). However, the lack of significant LREE enrichment, the strong HFSE depletion, and the N-MORB-like ε_{Nd} values of the Kamchatka lavas are significant differences from most modern arc shoshonites (e.g. Gill & Whelan, 1989).

Our mineralogical data indicate some heterogeneity of the magmatic system at the earliest stages of melt evolution. These include olivine phenocryst compositions (zoning and low- and high-Ca content) and occurrence of clinoenstatite as inclusions in low-Ca olivine. This heterogeneity exists in the ultramafic lavas from all localities studied, but is most

strongly developed in VR. These data strongly suggest mixing of different primitive magmas during early crystallization of olivine and spinel in shallow magma chambers. We suggest that the most magnesian low-Ca olivine may have originated from low-Ca boninite-like, clinoenstatite-bearing melts (Crawford *et al.*, 1989), whereas later crystallization of clinopyroxene was from a more homogenized magma, as shown by compositions of melt inclusions in clinopyroxene (Fig. 10).

The Kamchatka high-K ultramafic suite is an unusual end-member of the high-K island arc magmatic spectrum. Geochemical features of this magma type include high K_2O/Na_2O; enrichment in LILE, P and H_2O; low REE and HFSE contents combined with a weak relative enrichment or depletion in LREE and strong depletion in most incompatible HFSE (Nb and Ta); N-MORB-like ε_{Nd}; and Sr isotope values somewhat above the N-MORB range. These geochemical features are very consistent with the observation that low Ce/Yb magmas with high LILE/REE and high LILE/HFSE values tend to have more restricted and more depleted isotope compositions (Hawkesworth *et al.*, 1991, 1993), though this fact needs to be explained.

Geochemical characteristics of arc magmas, characterized by high LILE/HFSE and LILE/LREE, are traditionally explained as resulting from melting of depleted mantle peridotite affected by a metasomatic event generally believed to involve interaction with subduction-related $H_2O \pm CO_2$-bearing fluid or/and melt ('damp' component). The negative anomalies of Nb (Ta), Zr (Hf) and Ti of Kamchatka melts form a very depleted pattern typical for multiply melted, refractory peridotite and, therefore, may reflect the inherent property of the mantle wedge before the effects of subduction, assuming that these elements were not imported by metasomatic agents (McCulloch & Gamble, 1991; Maury *et al.*, 1992; Eggins, 1993). Possibly, the mantle peridotite source of the Kamchatka ultramafic rocks was more depleted than N-MORB mantle, and contributed refractory components and the volumetric bulk of magmas, whereas the 'damp' component was responsible for the gross input of the incompatible elements such as LILE, LREE, P and volatiles. As the majority of Nd and Sr appears to be contributed by metasomatism of the mantle wedge, the isotopic constraints may help to identify the source of the 'damp' component. The Nd isotope values of Kamchatka picrites are typical of those for North Pacific N-MORB (Hegner & Tatsumoto, 1987; White *et al.*, 1987), whereas $^{87}Sr/^{86}Sr$ ratios are markedly shifted to the right border of the mantle array, but still are within the field defined for MORB. The evident conflict between time-integrated depletion of the source and its enriched geochemistry can be resolved if we invoke partial melts of altered oceanic crust of depleted N-MORB composition as a possible source of the 'damp' component.

The ultramafic and associated mafic volcanics of Eastern Kamchatka make up a large volume of extrusive, subvolcanic and plutonic rocks. Geochemically similar rocks of the same age are known from Karaginsky Island in the Bering Sea (Sidorov, 1987) and from the Olutorskaya zone of the Koryak highland, to the north of Kamchatka (Fedorov & Kazimirov, 1989). Thus this magma type is relatively widespread in the Kamchatka region, at least within the Cretaceous successions. This high-K picritic magma type has also been described from several SW Pacific arcs of Late Cenozoic age, including Vanuatu (Gorton, 1977; Eggins, 1993), New Georgia in the Solomon arc (Ramsay *et al.*, 1984) and Fiji (Gill & Whelan, 1989). Although significant regional differences in trace element and isotopic compositions exist among these high-K picritic suites, more important is the demonstration that ultramafic magmas derived from upper-mantle peridotite have been erupted over Phanerozoic time.

ACKNOWLEDGEMENTS

We are grateful to V. P. Zinkevich and V. K. Gavrilov for assistance in field-work and stimulating discussions. Maxim Portnyagin took part in experimental studies and sample preparation. K. T. M. Johnson made ion-probe analyses of melt inclusions, N. Kononkova assisted with the electron-probe study. We gratefully acknowledge Tony Crawford for his thorough editing and help in recasting this paper into better English. The paper was greatly improved by critical reviews and helpful comments by T. J. Falloon and A. J. Crawford. V. S. K. thanks Leonid Danyushevsky for friendship and help during field-work, and Maya Kamenetsky for her assistance and encouragement. This work was supported by International Science Foundation (Grant MNN000) and by Russian Basic Research Foundation (Grant 93-05-8895).

REFERENCES

Arndt, N. T., 1986. Differentiation of komatiite flows. *Journal of Petrology* 27, 279–301.

Arndt, N. T. & Nisbet, E. G. (eds), 1982. *Komatiites*. London: George Allen & Unwin.

Arndt, N. T. & Nisbet, E. G., 1982. What is komatiite? In: Arndt, N. T. & Nisbet, E. G. (eds) *Komatiites*. London: George Allen & Unwin, pp. 19–27.

Burnham, C. W., 1975. Water and magmas: a mixing model. *Geochimica et Cosmochimica Acta* **39**, 1077–1082.

Byers, C. D., Christie, D. J., Muenow, D. W. & Sinton, J. M., 1984. Volatile contents and ferric–ferrous ratios of basalt, ferrobasalt, andesite and rhyodacite glasses from the Galapagos 95·5°W propagating rift. *Geochimica et Cosmochimica Acta* **48**, 2239–2245.

Byers, C. D., Garcia, M. O. & Muenow, D. W., 1985. Volatiles in pillow rim glasses from Loihi and Kilauea volcanoes, Hawaii. *Geochimica et Cosmochimica Acta* **49**, 1887–1896.

Byers, C. D., Garcia, M. O. & Muenow, D. W., 1986. Volatiles in basaltic glasses from the East Pacific Rise at 21°N: implications for MORB sources and submarine lava flow morphology. *Earth and Planetary Science Letters* **79**, 9–20.

Byers, C. D., Muenow, D. W. & Garcia, M. O., 1983. Volatiles in basalts and andesites from the Galapagos spreading center, 85° to 86°W. *Geochimica et Cosmochimica Acta* **47**, 1551–1558.

Chayla, B., Jaffrezic, H. & Joron, J.-L., 1973. Analyse par activation dans les mentions épithermiques. Application à la détermination d'éléments en trace dans les roches. *Comptes Rendus Hebdomadaires des Séances de l'Académie des Sciences* **277**, 273–275.

Clocchiatti, R., 1993. Les inclusions vitreuses et leur intérêt en magmatologie. *Mémoires de la Société Géologique de France* **163**, 57–67.

Crawford, A. J., 1980. A clinoenstatite-bearing cumulate olivine pyroxenite from Howqua, Victoria. *Contributions to Mineralogy and Petrology* **75**, 353–367.

Crawford, A. J., Falloon, T. J. & Green, D. H., 1989. Classification, petrogenesis and tectonic setting of boninites. In: Crawford, A. J. (ed.) *Boninites*. London: Unwin Hyman, pp. 1–49.

Dallwitz, W. B., Green, D. H. & Thompson, J. E., 1966. Clinoenstatite in volcanic rock from the Cape Vogel area, Papua. *Journal of Petrology* **7**, 375–403.

Danyushevsky, L. V., Falloon, T. J., Sobolev, A. V., Crawford, A. J., Carroll, M. & Price, R. C., 1993. The H_2O content of basalt glasses from Southwest Pacific back-arc basins. *Earth and Planetary Science Letters* **117**, 347–362.

Danyushevsky, L. V., Sobolev, A. V. & Kononkova, N. N., 1992. Methods of studying magma inclusions in minerals during investigations on water-bearing primitive mantle melts (Tonga Trench boninites). *Geochemistry International* **29**(7), 48–62.

DePaolo, D. J. & Johnson, R. W., 1979. Magma genesis in the New Britain island-arc: constraints from Nd and Sr isotopes and trace-element patterns. *Contributions to Mineralogy and Petrology* **70**, 367–379.

Duke, J. M., 1976. Distribution of the period four transition elements among olivine, calcic clinopyroxene and mafic silicate liquid: experimental results. *Journal of Petrology* **17**, 499–521.

Echeverría, L. M., 1980. Tertiary or Mesozoic komatiites from Gorgona island, Colombia: field relations and geochemistry. *Contributions to Mineralogy and Petrology* **73**, 253–266.

Eggins, S. M., 1993. Origin and differentiation of picritic arc magmas, Ambae (Aoba), Vanuatu. *Contributions to Mineralogy and Petrology* **114**, 79–100.

Erlikh, E. N., Shantser, A. E. & Kutyev, F. Sh., 1971. Meimechites of eastern Kamchatka. *Izvestiya Akademii Nauk SSSR, Seriya Geologicheskaya* **2**, 3–10 (in Russian).

Falloon, T. J. & Green, D. H., 1986. Glass inclusions in magnesian olivine phenocrysts from Tonga: evidence for highly refractory parental magmas in the Tongan arc. *Earth and Planetary Science Letters* **81**, 95–103.

Falloon, T. J. & Green, D. H., 1987. Anhydrous partial melting of MORB pyrolite and other peridotite compositions at 1 kbar: implications for the origin of primitive MORB glasses. *Mineralogy and Petrology* **37**, 181–219.

Falloon, T. J. & Green, D. H., 1988. Anhydrous partial melting of peridotite from 8 to 35 kbar and the petrogenesis of MORB. *Journal of Petrology, Special Lithosphere Issue*, 379–414.

Falloon, T. J., Green, D. H., Hatton, C. J. & Harris, K. L., 1988. Anhydrous partial melting of fertile and depleted peridotite from 2 to 30 kb and application to basalt petrogenesis. *Journal of Petrology* **29**, 1257–1282.

Falloon, T. J., Green, D. H. & McCulloch, M. T., 1989. Petrogenesis of high-Mg and associated lavas from the north Tonga trench. In: Crawford, A. J. (ed.) *Boninites*. London: Unwin Hyman, pp. 357–395.

Fedorov, P. I. & Kazimirov, A. D., 1989. Mineralogy and geochemistry of island-arc picrites (exemplified by southern Oliutor zone of Koryak upland). *Doklady Akademii Nauk SSSR* **306**, 456–460 (in Russian).

Ford, C. E., Russel, D. G., Graven, J. A. & Fisk, M. R., 1983. Olivine–liquid equilibria: temperature, pressure and composition dependence of the crystal/liquid cation partition coefficients for Mg, Fe^{2+}, Ca and Mn. *Journal of Petrology* **24**, 256–265.

Gill, J. B. & Whelan, P. M., 1989. Early rifting of an oceanic island arc (Fiji) produced shoshonitic to tholeiitic basalts. *Journal of Geophysical Research* **94**, 4561–4578.

Gorton, M. P., 1977. The geochemistry and origin of Quaternary volcanism in the New Hebrides. *Geochimica et Cosmochimica Acta* **41**, 1257–1270.

Hawkesworth, C. J., Gallagher, K., Hergt, J. M. & McDermott, F., 1993. Mantle and slab contributions in arc magmas. *Annual Review of Earth and Planetary Science* **21**, 175–204.

Hawkesworth, C. J., Hergt, J. M., McDermott, F. & Ellam, R. M., 1991. Destructive margin magmatism and the contributions from the mantle wedge and subducted crust. *Australian Journal of Earth Sciences* **38**, 577–594.

Hegner, E. & Tatsumoto, M., 1987. Pb, Sr and Nd isotopes in basalts and sulfides from the Juan de Fuca Ridge. *Journal of Geophysical Research* **92**, 11380–11386.

Hirose, K. & Kushiro, I., 1993. Partial melting of dry peridotites at high pressures—determination of compositions of melts segregated from peridotite using aggregates of diamond. *Earth and Planetary Science Letters* **114**, 477–489.

Jarosewich, E., Nelen, J. A. & Norberg, J. A., 1980. Reference samples for electron microprobe analysis. *Geostandards Newsletter* **4**, 43–47.

Johnson, K. T. M., 1990. Trace element geochemistry of oceanic peridotites and silicate melt inclusions: implications for mantle melting and ocean ridge magma genesis. Ph.D. Thesis, Woods Hole Oceanographic Institution–Massachusetts Institute of Technology.

Kamenetsky, V. S., Danyushevsky, L. V., Zinkevich, V. P., Tsukanov, N. V. & Romashova, T. V., 1991. New data on the picrites in the Cape Sharom Hills, Kamchatka. *Geochemistry International* **28**(11), 133–140.

Kamenetsky, V. S., Portnyagin, M. V., Sobolev, A. V. & Danyushevsky, L. V., 1993. Magma composition and crystallization conditions of the picrite–basalt suite in the Tumrok Ridge, East Kamchatka. *Geochemistry International* **30**(3), 58–73.

Karpenko, S. F., Sobolev, A. V., Kamenetsky, V. S., Danyushevsky, L. V., Makarova, T. I. & Lyalikov, A. V., 1989.

Isotope compositions of Nd and Sr of ultramafic volcanics of East Kamchatka. In: *Stable Isotopes in Geochemistry*, 12th Symp. Abstr. Moscow: Vernadsky Institute of Geochemistry, pp. 341–342 (in Russian).

Landa, E. A., Lyapunov, S. M. & Markovsky, B. A., 1983. On the peculiarities of rare-earth elements distribution in volcanic ultramafites. *Doklady Akademii Nauk SSSR* **272**, 462–464 (in Russian).

Lavrent'ev, Y. G., Pospelova, L. N. & Sobolev, N. V., 1974. Rock-forming mineral compositions determination by X-ray microanalysis. *Zavodskaya Laboratoriya* **40**, 657–666 (in Russian).

Letterrier, J., Maury, R. C., Thonon, P., Girard, D. & Marchal, M., 1982. Clinopyroxene composition as a method of identification of the magmatic affinities of paleo-volcanic series. *Earth and Planetary Science Letters* **59**, 139–154.

Luhr, J. F. & Carmichael, I. S. E., 1985. Jorullo Volcano, Michoacan, Mexico (1759–1774): the earliest stages of fractionation in calc-alkaline magmas. *Contributions to Mineralogy and Petrology* **90**, 142–161.

Markovsky, B. A. & Rotman, V. K., 1981. *Geology and Petrology of Ultramafic Volcanism*. Leningrad: Nedra (in Russian).

Maurel, C. & Maurel, P., 1982. Etude expérimentale de l'équilibre Fe^{2+}–Fe^{3+} dans les spinelles chromifières et les liquides silicates basiques coexistants, à 1 atm. *Comptes Rendus Hebdomadaires de l'Académie des Sciences* **295**, 209–212.

Maury, R. C., Defant, M. J. & Joron, J.-L., 1992. Metasomatism of the sub-arc mantle inferred from trace elements in Philippine xenoliths. *Nature* **360**, 661–663.

McCulloch, M. T. & Gamble, J. A., 1991. Geochemical and geodynamical constraints on subduction zone magmatism. *Earth and Planetary Science Letters* **102**, 358–374.

Metrich, N. & Clocchiatti, R., 1989. Melt inclusion investigation of the volatile behavior in historic alkali basaltic magmas of Etna. *Bulletin of Volcanology* **51**, 185–198.

Nisbet, E. G., 1982. The tectonic setting and petrogenesis of komatiites. In: Arndt, N. T. & Nisbet, E. G. (eds) *Komatiites*. London: George Allen & Unwin, pp. 501–520.

Perfit, M. R., Gust, D. A., Bence, A. E., Arculus, R. J. & Taylor, S. R., 1980. Chemical characteristics of island-arc basalts: implications for mantle sources. *Chemical Geology* **30**, 227–256.

Ramsay, W. R. H., Crawford, A. J. & Foden, J. D., 1984. Field setting, mineralogy, chemistry, and genesis of arc picrites, New Georgia, Solomon Islands. *Contributions to Mineralogy and Petrology* **88**, 386–402.

Roedder, E., 1984. *Fluid Inclusions*. Chelsea, MI: Book-Crafters.

Roeder, P. L. & Emslie, R. F., 1970. Olivine–liquid equilibrium. *Contributions to Mineralogy and Petrology* **29**, 275–289.

Seliverstov, V. A., 1978. Ophiolites of Eastern Kamchatka. In: *Petrological Investigations of Island-Arc Basic Rocks*. Moscow: Institute of Earth Physics, pp. 177–239 (in Russian).

Seliverstov, V. A., Koloskov, A. V., Laputina, I. P., Philosophova, T. M. & Chubarov, V. M., 1984. First data on the composition of minerals of the deep-seated inclusions in the meimechites of Kamchatka. *Doklady Akademii Nauk SSSR* **278**, 949–953 (in Russian).

Sidorov, E. G., 1987. Find of picrites in the Karaginsky Island (Bering Sea). *Doklady Akademii Nauk SSSR* **297**, 681–683 (in Russian).

Sigurdsson, I. A., Kamenetsky, V. S., Crawford, A. J., Eggins, S. M. & Zlobin, S. K., 1993. Primitive island arc and oceanic lavas from the Hunter Ridge–Hunter Fracture Zone. Evidence from glass, olivine and spinel composition. *Mineralogy and Petrology* **47**, 149–169.

Sobolev, A. V. & Chaussidon, M., 1995. The H_2O contents in the primary mantle derived magmas: evidence from SIMS analyses of melt inclusions in high-magnesian olivines. *Earth and Planetary Science Letters* (submitted).

Sobolev, A. V. & Danyushevsky, L. V., 1994. Petrology and geochemistry of boninites from the north termination of the Tonga Trench: constraints on the generation conditions of primary high-Ca boninite magmas. *Journal of Petrology* **35**, 1183–1211.

Sobolev, A. V., Dmitriev, L. V., Barsukov, V. L., Nevsorov, V. N. & Slutsky, A. B., 1980. The formation conditions of high-magnesium olivines from the monomineralic fraction of Luna 24 regolith. *Proceedings of the 11th Lunar and Planetary Science Conference*. Oxford: Pergamon, pp. 105–116.

Sobolev, A. V., Kamenetsky, V. S. & Kononkova, N. N., 1990. Petrology and geochemistry of ultramafic volcanites of Valaga Ridge (East Kamchatka). *Geochemistry International* **27**(7), 1694–1709.

Sobolev, A. V., Kamenetsky, V. S. & Kononkova, N. N., 1992. New data on Siberian meymechite petrology. *Geochemistry International* **29**(3), 10–20.

Sobolev, A. V., Kamenetsky, V. S., Metrich, N., Clocchiatti, R., Kononkova, N. N., Devirts, A. L. & Ustinov, V. I., 1991. Volatile regime and crystallization conditions in Etna hawaiite lavas. *Geochemistry International* **28**(4), 53–65.

Sobolev, A. V., Portnyagin, M. V., Dmitriev, L. V., Tsameryan, O. P., Danyushevsky, L. V., Kononkova, N. N., Shimizu, N. & Robinson, P. T., 1993. Petrology of ultramafic lavas and associated rocks of the Troodos massif, Cyprus. *Petrology* **1**, 331–361.

Sobolev, A. V. & Slutsky, A. B., 1984. Composition and crystallization conditions of the initial melt of the Siberian meimechites in relation to the general problem of the ultrabasic magmas. *Soviet Geology and Geophysics* **25**, 93–104 (in Russian).

Sun, S.-S. & McDonough, W. F., 1989. Chemical and isotopic systematics of oceanic basalts: implications for mantle composition and processes. In: Saunders, A. D. & Norry, M. J. (eds). *Magmatism in the Ocean Basins. Geological Society Special Publication* **42**, 313–345.

Takahashi, E., 1986. Melting of a dry peridotite KLB-1 up to 14 GPa: implications for the origin of peridotitic upper mantle. *Journal of Geophysical Research* **91**, 9367–9382.

Takahashi, E. & Kushiro, I., 1983. Melting of a dry peridotite at high pressures and basalt magma genesis. *American Mineralogist* **68**, 859–879.

Takahashi, E. & Scarfe, C. M., 1985. Melting of peridotite to 14 GPa and genesis of komatiite. *Nature* **315**, 566–568.

Walker, D. A. & Cameron, W. E., 1983. Boninite primary magmas: evidence from Cape Vogel Peninsula, Papua New Guinea. *Contributions to Mineralogy and Petrology* **83**, 150–158.

Wendlandt, R. F. & Eggler, D. H., 1977. Phase relations of a kimberlite. *Carnegie Institution of Washington, Yearbook* **77**, 751–756.

White, W. M., Hofmann, A. W. & Puchelt, H., 1987. Isotope geochemistry of Pacific mid-ocean ridge basalts. *Journal of Geophysical Research* **92**, 4881–4893.

Zinkevich, V. P., Danyushevsky, L. V., Kamenetsky, V. S., Konstantinovskaya, E. A., Magakyan, R., Seliverstov, V. A. & Portnyagin, M. V., 1991. Geology and geochemistry of Cretaceous and Paleogene volcanics of Tumrok range (East Kamchatka). *Tikhookeanskaya Geologiya* **5**, 84–99 (in Russian).

Zinkevich, V. P., Konstantinovskaya, E. A., Magakyan, R. & Tsukanov, N. V., 1989. Tectonic nappes of the northern part of

Valaginsky Range (East Kamchatka). *Tikhookeanskaya Geologiya* **3**, 62–71 (in Russian).

Zinkevich, V. P., Konstantinovskaya, E. A., Magakyan, R. & Tsukanov, N. V., 1990. Accretion structure of East Kamchatka. *Doklady Akademii Nauk SSSR* **312**, 1186–1190 (in Russian).

Zlobin, S. K., Kamenetsky, V. S., Sobolev, A. V. & Kononkova, N. N., 1991. Chrome spinel inclusion data on the parent melt for the parallel-dike complex in the Mainits-zone ophiolites in the Koryak uplands. *Geochemistry International* 28(6), 68–77.

RECEIVED JANUARY 4, 1994
REVISED TYPESCRIPT ACCEPTED OCTOBER 3, 1994